ACADEMIC PRESS

Available online at www.sciencedirect.com

SCIENCE DIRECT®

ICARUS

Icarus 161 (2003) 262–280

www.elsevier.com/locate/icarus

Compositional analyses of lunar pyroclastic deposits

Lisa R. Gaddis,[a,*] Matthew I. Staid,[a] James A. Tyburczy,[b] B. Ray Hawke,[c] and Noah E. Petro[d,1]

[a] *Astrogeology Program, U.S. Geological Survey, 2255 N. Gemini Drive, Flagstaff, AZ 86001, USA*
[b] *Department of Geological Sciences, Arizona State University, Tempe, AZ 85282, USA*
[c] *HIGP/SOEST, University of Hawaii at Manoa, 2525 Correa Road, Honolulu, HI 96822, USA*
[d] *Bates College, Lewiston, ME 04240, USA*

Received 21 May 2002; revised 10 September 2002

Abstract

The 5-band Clementine UVVIS data at ~100 m/pixel were used to examine the compositions of 75 large and small lunar pyroclastic deposits (LPDs), and these were compared to representative lunar maria and highlands deposits. Results show that the albedo, spectral color, and inferred composition of most LPDs are similar to those of low-titanium, mature lunar maria. These LPDs may have consisted largely of fragmented basalt, with substantial components of iron-bearing mafic minerals (pyroxenes, olivine) and smaller amounts (if any) of volcanic glass. Several smaller LPDs also show substantial highland components. Three classes of very large deposits can be distinguished from most LPDs and from each other on the basis of crystallinity and possible titanium content of their pyroclastic components. One class has spectral properties that are dominated by high-titanium, crystallized "black beads" (e.g., Taurus–Littrow), a second consists of a mixture of high-titanium glasses and beads with a higher glass/bead ratio (Sulpicius Gallus) than that of Taurus–Littrow, and a third has a significant component of quenched iron-bearing volcanic glasses (Aristarchus) with possible moderate titanium contents. Although areally extensive, these three classes of very large pyroclastic deposits compose only 20 of the 75 deposits studied (~27%), and eruption of such materials was thus likely to have been less frequent on the Moon.

Keywords: Moon; Moon surface; Volcanism; Spectroscopy

I. Introduction

Lunar pyroclastic deposits are low-albedo units that are thought to mark the source regions of ancient volcanic eruptions on the Moon (Head, 1974). Quenched iron-bearing glass and crystallized beads with volatile-element coatings are major components of several of the larger pyroclastic deposits (e.g., Pieters et al., 1973, 1974; Adams et al., 1974; Heiken et al., 1974; Gaddis et al., 1985). Laboratory analyses of picritic volcanic glass samples from several of these deposits show that the glasses had a greater depth of origin and lesser fractional crystallization than lunar mare basalts (Delano, 1986; Shearer and Papike, 1993; Papike et al., 1998). These data indicate that volcanic glasses are the best examples of primitive materials on the Moon, and they are of critical importance both in characterizing the lunar interior and as a starting place for understanding the origin and evolution of lunar basaltic magmatism. Several smaller LPDs are known to have spectral properties similar to those of lunar highland and mare deposits and both volcanic glass and olivine have been cited as additional juvenile components (e.g., Hawke et al., 1989a, 1989b), but the compositions of the majority of LPDs have not been studied in detail. Characterization of the nature of the lunar pyroclastic deposits (LPDs), particularly the compositions of their most primitive juvenile compo-

* Corresponding author. Fax: +1-928-556-7014.
E-mail address: lgaddis@usgs.gov (L.R. Gaddis).
[1] Present address: Dept. of Geological Sciences, Box 1846, Brown University, Providence, RI 02912, USA.

0019-1035/03/$ – see front matter © 2003 Elsevier Science (USA). All rights reserved.
doi:10.1016/S0019-1035(02)00036-2

nents, is essential for models of the formation, segregation, and emplacement of lunar magmas.

Earth-based remote sensing analyses of several of the larger LPDs have helped to identify their pyroclastic components (e.g., Adams et al., 1974; Pieters et al., 1973, 1974; Gaddis et al., 1985; Weitz et al., 1998; Gaddis et al., 2000) and to characterize these iron-, titanium-, and volatile-element-enriched materials as potential resource materials for future exploitation (Hawke et al., 1990; Allen et al., 1996; Coombs et al., 1998). These data also helped to constrain the spatial distribution of early lunar volcanic deposits (Head, 1974) and to understand the styles of eruption and emplacement of basalts on the Moon (Wilson and Head, 1981). To fully appreciate the role of pyroclastic volcanism in the context of basaltic volcanism on the Moon we must understand the spatial and temporal distribution, relationship to other volcanic deposits, range of compositions, and modes of occurrence and formation of LPDs. Until additional samples are available, remote analyses of lunar pyroclastic deposits are a primary means of characterizing these deposits. This paper presents an analysis of the application of the global 5-band Clementine ultraviolet–visible (UVVIS) multispectral data (Eliason et al., 1999) to characterization of the compositions of lunar pyroclastic deposits. To establish geologic context, this paper first briefly reviews the current state of knowledge of the morphology, spatial extent, distribution, age, physical nature, and compositions for several LPDs as derived from both laboratory analyses of samples and Earth-based spectral data.

II. Characteristics of lunar pyroclastic deposits

More than 100 lunar pyroclastic deposits have been mapped (Wilhelms and McCauley, 1971; Scott et al., 1977; Wilhelms and El-Baz, 1977; Lucchitta, 1978; Wilhelms et al., 1979) and described (e.g., Gaddis et al., 1985; Coombs and Hawke, 1992; Coombs et al., 1990a, 1990b; Hawke et al., 1979, 1989a, 1991; Gaddis et al., 1997, 1998a, 1998b, 1999, 2000; Rosanova et al., 1998). Ongoing Clementine-based geologic analyses of the Moon will no doubt continue to identify new deposits (e.g., Heather et al., 2001). This paper addresses remote characterization of the compositions of 75 deposits that have been most frequently identified as pyroclastic in the literature and on published maps (Tables 1 and 2). The sections below summarize the characteristics of these deposits.

II.A. Morphology

LPDs are generally observed as dark deposits in the highlands on the floors of craters and/or near mare deposits, and they are often associated with fractures, irregular depressions, non-circular craters, and other likely volcanic vents (Fig. 1). LPDs often appear to drape over or mantle the underlying surface, which may be flat mare, smooth plains, or hummocky highland deposits. LPDs may be relatively thick, subduing subjacent terrain, or they may occur as thin mantles with frequent exposures of substrate.

Both thickness and geologic context of a deposit, especially the relative brightness of the substrate or other local material, can influence the apparent albedo of a LPD. For example, the numerous knobs of subjacent highland material that are observed within the Orientale LPD indicate that this deposit is relatively thin (<2 m; Head et al., 2002). The superposition of brighter materials, such as crater rays, can also artificially brighten an LPD. An example of such a case is seen in the eastern floor of the Nectarian crater Oppenheimer (Fig. 1, bottom), where several LPDs have been brightened by the superposition of high-albedo rays from the younger Copernican crater Jackson (71 km dia.) to the north.

Although most LPDs are readily recognized on the basis of their low albedo, mantling appearance, and/or association with a volcanic vent, identification and characterization of LPDs are problematic in some areas. For example, at a single vent both explosively and fluidly emplaced volcanic materials may be present, and these deposits may not be distinguishable on the basis of differences in albedo, surface texture, or composition (e.g., in places on the Compton crater floor and in the Moscoviense region). These difficulties may result in an incorrect estimation of the number of LPDs and/or mare ponds identified. Larger deposits may be underrepresented in the population of recognized LPDs because of erroneous assessment of the areal extent or size due to obscuration by a younger volcanic deposit. Although mapped as pyroclastic in the past, as many as 8 of the 75 ($\sim$10.7%) LPDs studied here (e.g., Lubiniezky, Hell, Airy) do not have very low albedos or identifiable vents and thus they may be mare ponds or some other type of smooth-surfaced lunar deposits (e.g., smooth plains, impact melts).

II.B. Distribution

LPDs are widely distributed across the Moon (Fig. 2) and they are commonly observed in the highlands along the margins of or within most major basins with mare fill. Smaller pyroclastic deposits are observed both in proximity to mare deposits (e.g., Moscoviense, Schrodinger) and in relative isolation from other volcanic deposits (e.g., Oppenheimer). In the latter case, smaller LPDs are commonly found in the floors of floor-fractured craters, where they are often associated with endogenic craters aligned along one or more fractures. Of more than 80 floor-fractured craters mapped by Wilhelms (1987), 16 (20%) have associated small pyroclastic deposits.

The spatial association of volcanic eruption sites and impact craters and basins on the Moon is well known and is believed to be related to crustal thinning beneath impact sites (e.g., Head and Wilson 1979). Like the lunar maria, LPDs are observed over a wide range of crustal thickness as derived from the Clementine lidar data (e.g., Zuber et al.,

Table 1
Lunar pyroclastic deposits: location, size classification, and geologic setting

No.	Site	Latitude (°)	Longitude (°)	Area (km^2)	Size class	Geologic setting
1	Aristarchus	26.7	−52.3	49013	vlarge	Mantled highlands plateau near mare/highland boundary
2	Aestuum	6.6	−5.9	10357	vlarge	Mantled highlands near mare/highland boundary
3	Rima Bode	11.9	−3.4	6620	vlarge	Mantled highlands near mare/highland boundary
4	Smythii NW	1.1	84.8	5851	vlarge	Mantled highlands on basin floor
5	Orientale	−30.3	−97.5	5321	vlarge	Mantled highlands, aureole form on basin rim
6	Cruger	−16.7	−66.5	4828	vlarge	Mantled highlands
7	Sulpicius Gallus	21.7	9.4	4322	vlarge	Mantled highlands near mare/highland boundary on basin rim
8	Vaporum	10.0	7.9	4129	vlarge	Mantled highlands near mare/highland boundary
9	Taurus–Littrow	20.2	30.7	2940	vlarge	Mantled mare near mare/highland boundary on basin rim
10	Nectaris SE	−22.4	40.5	2905	vlarge	Mantled highlands near basin
11	Harbinger	26.6	−43.4	2877	vlarge	Mantled highlands near mare/highland boundary
12	Dopplemayer	−28.1	−40.5	2628	vlarge	Mantled highlands on basin floor near mare/highland boundary
13	Smythii SW	−6.0	85.0	2539	vlarge	Mantled highlands on basin floor
14	Titius	−26.7	103.9	2159	vlarge	Mantled highlands
15	Petavius	−23.5	61.0	1645	vlarge	Mantled highlands on crater floor, poss, assoc. mare pond
16	Oppenheimer NW	−34.8	−168.2	1500	vlarge	Mantled highlands on crater floor
17	Humorum SW	−26.6	−44.4	1472	vlarge	Mantled highlands on basin floor near mare/highland boundary
18	Riccioli	−2.4	−75.5	1089	vlarge	Mantled highlands
19	Cleomedes	26.6	54.7	1084	vlarge	Mantled highlands on crater floor, poss. assoc. mare pond
20	Moscoviense SE	24.7	151.2	1022	vlarge	Mantled highlands on basin floor near mare/highland boundary
21	Hadley Cleft	25.2	2.6	898	large	Mantled mare on basin floor near mare/highland boundary
22	Schrodinger	−75.4	138.6	819	large	Mantled smooth plains on basin floor
23	Taruntius NW	9.4	43.6	819	large	Mantled highlands near mare/highland boundary
24	Oppenheimer S	−37.9	−166.9	674	large	Mantled highlands on crater floor
25	J. Herschel	61.7	−36.6	666	large	Mantled highlands on crater floor
26	Beer	27.2	−8.0	623	large	Mantled highlands on basin floor near mare/highland boundary
27	Mozart	23.8	1.3	589	large	Mantled highlands on basin floor near mare/highland boundary
28	Lavoisier	38.2	−80.8	568	large	Mantled highlands on crater floor near mare/highland boundary
29	Lavoisier F	36.9	−80.6	553	large	Mantled highlands on crater floor near mare/highland boundary
30	Schluter	−10.3	−83.0	489	large	Mantled highlands
31	Barnard	−31.3	89.0	444	large	Mantled highlands on crater floor
32	Frigoris SE/W	49.6	27.5	444	large	Mantled highlands near mare/highland boundary
33	Cavalerius	6.4	−66.4	428	large	Mantled highlands near mare/highland boundary
34	Briggs A	28.6	−74.2	415	large	Mantled highlands near mare/highland boundary
35	Gaudibert	−12.3	38.6	400	large	Mantled highlands on basin floor near mare/highland boundary
36	Carpatus	14.6	−25.4	354	medium	Mantled highlands on basin rim near mare/highland boundary
37	Daguerre	−11.3	34.1	323	medium	Mantled highlands on basin floor near mare/highland boundary
38	Fresnel	28.2	4.4	307	medium	Mantled highlands on basin floor near mare/highland boundary
39	Humboldt SW	−28.5	78.8	277	medium	Mantled highlands on crater floor, poss, assoc. mare pond
40	Gauss S	34.2	78.7	263	medium	Mantled highlands on crater floor
41	Taruntius	5.1	46.2	250	medium	Mantled highlands on crater floor
42	Frigoris SE/E	50.2	34.4	244	medium	Mantled highlands near mare/highland boundary
43	Abel B	−36.6	82.4	236	medium	Mantled highlands on crater floor
44	Oppenheimer SW	−37.0	−168.3	227	medium	Mantled highlands on crater floor
45	Franklin	38.3	47.9	198	small	Mantled highlands on crater floor
46	Oppenheimer SE	−37.0	−163.4	194	small	Mantled highlands on crater floor
47	Lassell	−15.4	−7.9	192	small	Mantled highlands on crater floor
48	Abel C	−36.1	81.0	191	small	Mantled highlands on crater floor
49	Compton	54.1	105.1	182	small	Mantled highlands on crater floor, poss, assoc. mare pond
50	Gauss W	35.7	76.0	179	small	Mantled highlands on crater floor
51	Lagrange C	−29.5	−64.4	174	small	Mantled highlands on crater floor
52	Lubinieszky	−17.1	−24.6	170	small	Mantled highlands near mare/highland boundary
53	Humboldt NE	−25.8	82.9	169	small	Mantled highlands on crater floor, poss. assoc. mare pond
54	Atlas S	45.7	44.6	147	small	Mantled highlands on crater floor
55	Atlas N	47.3	44.8	132	small	Mantled highlands on crater floor
56	Mersenius	−20.9	−49.9	129	small	Mantled highlands
57	Grimaldi	−0.8	−64.8	127	small	Mantled highlands near mare/highland boundary
58	Vitruvius	17.7	31.2	120	small	Mantled highlands on crater floor, near mare/highlands boundary
59	Messala S	40.1	59.3	116	small	Mantled highlands on crater floor
60	Daniell	35.4	31.1	100	small	Mantled plains on crater floor
61	Lavoisier H	37.9	−78.3	100	small	Mantled highlands on crater floor near mare/highland boundary
62	Alphonsus NNE	−12.8	−1.7	98	vsmall	Mantled highlands in floor-fractured crater
63	Alphonsus W	−13.6	−4.1	95	vsmall	Mantled highlands in floor-fractured crater
64	Humboldt W	−26.6	78.2	94	vsmall	Mantled highlands on crater floor
65	Gambart	1.9	−15.1	88	vsmall	Mantled highlands in maria
66	Alphonsus E	−14.3	−2.0	82	vsmall	Mantled highlands on crater floor
67	Gauss E	36.0	81.2	70	vsmall	Mantled highlands on crater floor
68	Humboldt NW	−25.1	78.9	69	vsmall	Mantled highlands on crater floor
69	Gaudibert NW	−11.1	37.7	62	vsmall	Mantled highlands on crater floor near mare/highlands boundary
70	Hell	−32.5	−7.7	57	vsmall	Mantled highlands on crater floor
71	Messala N	40.5	59.3	49	vsmall	Mantled highlands on crater floor
72	Apollo	−30.0	−153.1	42	vsmall	Mantled highlands on crater floor
73	Airy	−18.0	5.7	22	vsmall	Mantled highlands
74	Alphonsus Exo	−14.8	−2.3	10	vsmall	Mantled highlands on crater floor
75	Alphonsus C	−13.7	−3.4	3	vsmall	Mantled highlands on crater floor

Table 2
Lunar pyroclastic deposits: Clementine UVVIS color and color-ratio data

No.	Site	415/750 nm	950/750 nm	415 nm	415 nm error	750 nm	750 nm error	900 nm	900 nm error	950 nm	950 nm error	1000 nm	1000 nm error
1	Aristarchus	0.546	1.043	0.052	0.002	0.095	0.004	0.098	0.004	0.099	0.004	0.102	0.004
2	Aestuum	0.630	1.101	0.054	0.003	0.086	0.009	0.092	0.008	0.095	0.007	0.099	0.007
3	Rima Bode	0.610	1.090	0.050	0.002	0.082	0.004	0.087	0.004	0.090	0.004	0.094	0.004
4	Smythii NW	0.582	1.074	0.065	0.003	0.112	0.005	0.118	0.006	0.120	0.006	0.124	0.006
5	Orientale	0.582	1.087	0.084	0.007	0.145	0.011	0.154	0.011	0.157	0.011	0.163	0.011
6	Cruger	0.576	1.087	0.084	0.005	0.146	0.010	0.155	0.011	0.158	0.011	0.164	0.011
7	Sulpicius Gallus	0.588	1.089	0.051	0.004	0.086	0.007	0.092	0.007	0.094	0.007	0.098	0.007
8	Vaporum	0.620	1.094	0.049	0.002	0.079	0.003	0.084	0.003	0.086	0.003	0.089	0.003
9	Taurus–Littrow	0.637	1.100	0.055	0.001	0.086	0.002	0.093	0.002	0.095	0.002	0.099	0.003
10	Nectaris SE	0.595	1.080	0.083	0.005	0.140	0.006	0.148	0.006	0.151	0.007	0.155	0.007
11	Harbinger	0.545	1.017	0.058	0.003	0.106	0.004	0.108	0.005	0.108	0.005	0.111	0.005
12	Dopplemayer	0.581	1.052	0.056	0.002	0.097	0.002	0.101	0.002	0.102	0.003	0.105	0.003
13	Smythii SW	0.575	1.087	0.067	0.009	0.117	0.014	0.124	0.013	0.127	0.013	0.131	0.013
14	Titius	0.588	1.060	0.067	0.004	0.115	0.006	0.120	0.006	0.121	0.006	0.126	0.006
15	Petavius	0.623	1.039	0.094	0.005	0.151	0.005	0.155	0.005	0.156	0.005	0.160	0.006
16	Oppenheimer NW	0.578	1.059	0.054	0.002	0.093	0.004	0.097	0.004	0.098	0.004	0.103	0.004
17	Humorum SW	0.565	1.051	0.057	0.001	0.101	0.002	0.104	0.002	0.106	0.002	0.110	0.002
18	Riccioli	0.587	1.057	0.077	0.004	0.132	0.007	0.138	0.008	0.139	0.008	0.144	0.008
19	Cleomedes	0.581	1.022	0.090	0.006	0.154	0.011	0.156	0.012	0.157	0.011	0.163	0.013
20	Moscoviense SE	0.559	1.082	0.067	0.007	0.120	0.011	0.127	0.013	0.130	0.013	0.135	0.013
21	Hadley Cleft	0.567	1.054	0.070	0.007	0.124	0.010	0.128	0.010	0.130	0.010	0.135	0.010
22	Schrodinger	0.569	1.015	0.098	0.006	0.173	0.010	0.174	0.011	0.175	0.011	0.182	0.012
23	Taruntius NW	0.591	1.072	0.072	0.002	0.121	0.003	0.127	0.004	0.130	0.004	0.134	0.003
24	Oppenheimer S	0.574	1.063	0.058	0.004	0.101	0.007	0.106	0.007	0.108	0.007	0.112	0.007
25	J. Herschel	0.545	1.028	0.086	0.007	0.157	0.010	0.159	0.010	0.161	0.010	0.168	0.010
26	Beer	0.596	1.045	0.067	0.002	0.112	0.003	0.116	0.003	0.118	0.003	0.121	0.003
27	Mozart	0.581	1.049	0.073	0.003	0.125	0.004	0.129	0.004	0.132	0.004	0.137	0.004
28	Lavoisier	0.596	1.064	0.072	0.003	0.121	0.004	0.126	0.004	0.128	0.004	0.133	0.004
29	Lavoisier F	0.578	1.070	0.064	0.005	0.111	0.005	0.116	0.005	0.119	0.005	0.123	0.005
30	Schluter	0.588	1.061	0.083	0.002	0.142	0.003	0.149	0.003	0.150	0.003	0.155	0.003
31	Barnard	0.588	1.061	0.075	0.004	0.127	0.006	0.133	0.006	0.135	0.006	0.140	0.006
32	Frigoris SE/W	0.545	1.063	0.070	0.004	0.129	0.007	0.135	0.007	0.137	0.007	0.144	0.007
33	Cavalerius	0.587	1.059	0.068	0.001	0.117	0.001	0.122	0.001	0.123	0.001	0.128	0.001
34	Briggs A	0.589	1.022	0.080	0.002	0.135	0.005	0.138	0.005	0.138	0.005	0.142	0.006
35	Gaudibert	0.583	1.064	0.071	0.003	0.121	0.004	0.127	0.004	0.129	0.005	0.133	0.004
36	Carpatus	0.586	1.048	0.072	0.003	0.122	0.004	0.126	0.005	0.128	0.005	0.132	0.005
37	Daguerre	0.583	1.074	0.066	0.004	0.113	0.006	0.118	0.007	0.121	0.008	0.125	0.008
38	Fresnel	0.570	1.049	0.068	0.002	0.119	0.004	0.123	0.004	0.125	0.003	0.129	0.004
39	Humboldt SW	0.582	1.054	0.083	0.006	0.142	0.009	0.152	0.013	0.149	0.010	0.154	0.010
40	Gauss S	0.561	1.059	0.090	0.006	0.161	0.006	0.167	0.008	0.171	0.007	0.178	0.007
41	Taruntius	0.607	1.031	0.077	0.006	0.128	0.009	0.131	0.008	0.132	0.008	0.135	0.009
42	Frigoris SE/E	0.552	1.064	0.074	0.002	0.134	0.003	0.140	0.004	0.142	0.004	0.148	0.004
44	Abel B	0.564	1.100	0.080	0.002	0.141	0.003	0.151	0.003	0.156	0.003	0.161	0.003
44	Oppenheimer SW	0.569	1.049	0.055	0.001	0.096	0.002	0.099	0.002	0.101	0.002	0.105	0.002
45	Franklin	0.561	1.089	0.084	0.009	0.150	0.014	0.159	0.014	0.164	0.015	0.170	0.015
46	Oppenheimer SE	0.589	1.024	0.077	0.002	0.131	0.003	0.133	0.003	0.134	0.003	0.139	0.003
47	Lassell	0.619	1.017	0.071	0.002	0.115	0.002	0.117	0.001	0.117	0.001	0.120	0.002
48	Abel C	0.563	1.084	0.077	0.002	0.137	0.002	0.144	0.002	0.148	0.002	0.154	0.002
49	Compton	0.579	1.039	0.129	0.005	0.223	0.008	0.229	0.009	0.232	0.010	0.240	0.010
50	Gauss W	0.561	1.059	0.089	0.001	0.158	0.003	0.164	0.003	0.167	0.003	0.174	0.003
51	Lagrange C	0.582	1.034	0.090	0.003	0.155	0.005	0.159	0.006	0.160	0.007	0.166	0.007
52	Lubinieszky	0.595	1.012	0.077	0.002	0.129	0.003	0.131	0.003	0.131	0.004	0.134	0.004
53	Humboldt NE	0.598	1.058	0.085	0.005	0.141	0.009	0.147	0.009	0.150	0.009	0.152	0.007
54	Atlas S	0.572	1.077	0.080	0.003	0.140	0.007	0.146	0.009	0.150	0.010	0.157	0.010
55	Atlas N	0.560	1.056	0.090	0.009	0.160	0.014	0.166	0.015	0.169	0.016	0.176	0.017
56	Mersenius	0.577	1.070	0.079	0.002	0.137	0.004	0.144	0.004	0.147	0.004	0.152	0.004
57	Grimaldi	0.576	1.087	0.084	0.005	0.146	0.010	0.155	0.011	0.158	0.011	0.164	0.011
58	Vitruvius	0.632	1.033	0.067	0.001	0.105	0.003	0.108	0.003	0.109	0.003	0.112	0.003
59	Messala S	0.554	1.093	0.086	0.001	0.156	0.003	0.165	0.003	0.170	0.003	0.177	0.003
60	Daniell	0.555	1.051	0.071	0.002	0.128	0.003	0.132	0.003	0.134	0.004	0.140	0.004
61	Lavoisier H	0.585	1.079	0.062	0.001	0.107	0.003	0.113	0.003	0.115	0.004	0.121	0.003
62	Alphonsus NNE	0.568	1.050	0.079	0.005	0.139	0.008	0.144	0.008	0.146	0.008	0.151	0.009
63	Alphonsus W	0.562	1.039	0.069	0.002	0.122	0.003	0.126	0.004	0.127	0.004	0.132	0.004
64	Humboldt W	0.580	1.074	0.084	0.006	0.145	0.009	0.152	0.010	0.156	0.010	0.161	0.010
65	Gambart	0.592	1.052	0.060	0.003	0.102	0.003	0.106	0.003	0.107	0.003	0.110	0.003
66	Alphonsus E	0.562	1.041	0.071	0.001	0.126	0.001	0.130	0.001	0.131	0.002	0.136	0.001
67	Gauss E	0.567	1.068	0.101	0.004	0.179	0.006	0.186	0.007	0.191	0.007	0.198	0.008
68	Humboldt NW	0.579	1.082	0.079	0.001	0.136	0.001	0.144	0.001	0.147	0.001	0.152	0.001
69	Gaudibert NW	0.581	1.073	0.083	0.002	0.142	0.004	0.150	0.004	0.153	0.004	0.156	0.005
70	Hell	0.598	1.019	0.122	0.016	0.204	0.023	0.207	0.026	0.208	0.027	0.214	0.027
71	Messala N	0.557	1.092	0.087	0.007	0.157	0.011	0.166	0.011	0.171	0.011	0.178	0.011
72	Apollo	0.606	1.008	0.080	0.005	0.133	0.007	0.133	0.008	0.134	0.008	0.138	0.009
73	Airy	0.579	1.057	0.097	0.005	0.167	0.007	0.174	0.008	0.177	0.008	0.183	0.008
74	Alphonsus Exo	0.568	1.051	0.081	0.002	0.142	0.003	0.148	0.004	0.150	0.004	0.155	0.004
75	Alphonsus C	0.572	1.042	0.076	0.002	0.134	0.003	0.138	0.004	0.139	0.004	0.145	0.004

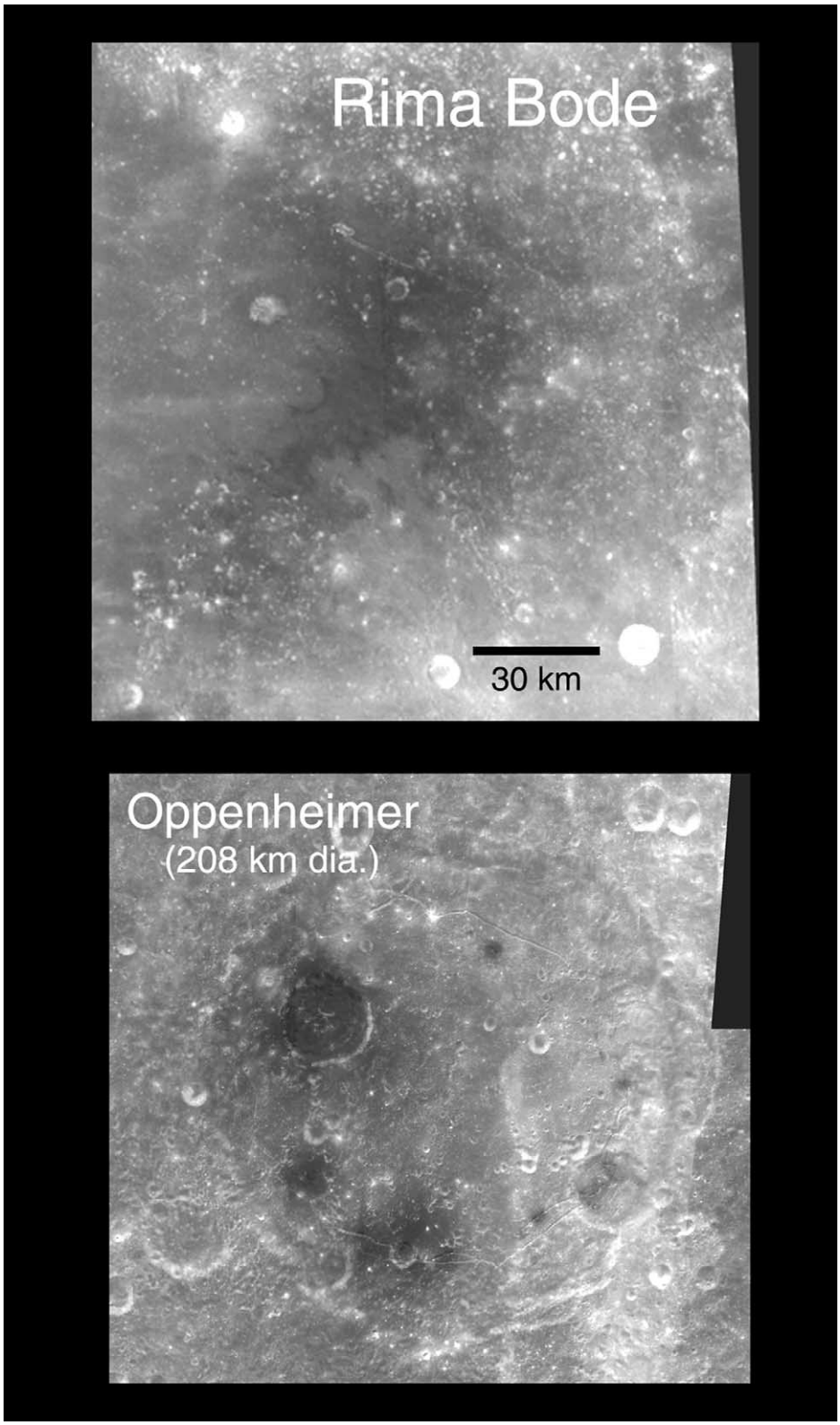

Fig. 1. Clementine 750-nm images of dark pyroclastic deposits at Rima Bode (top) and in the floor of Oppenheimer crater (bottom). See Fig. 2 and Table 1 for locations and more information. Note that Rima Bode is #3 and Oppenheimer deposits are #16, #24, #44, and #46 in Fig. 2 and Table 1.

1994). Most large LPDs are observed in regions with crustal thicknesses from ~50 to 75 km, and small pyroclastic deposits are observed in regions with crustal thicknesses ranging from 25 to 65 km (Gaddis et al., 1998a, 1998b). On the lunar near side, these crustal thicknesses are typical of the margins of the major maria. On the far side pyroclastic

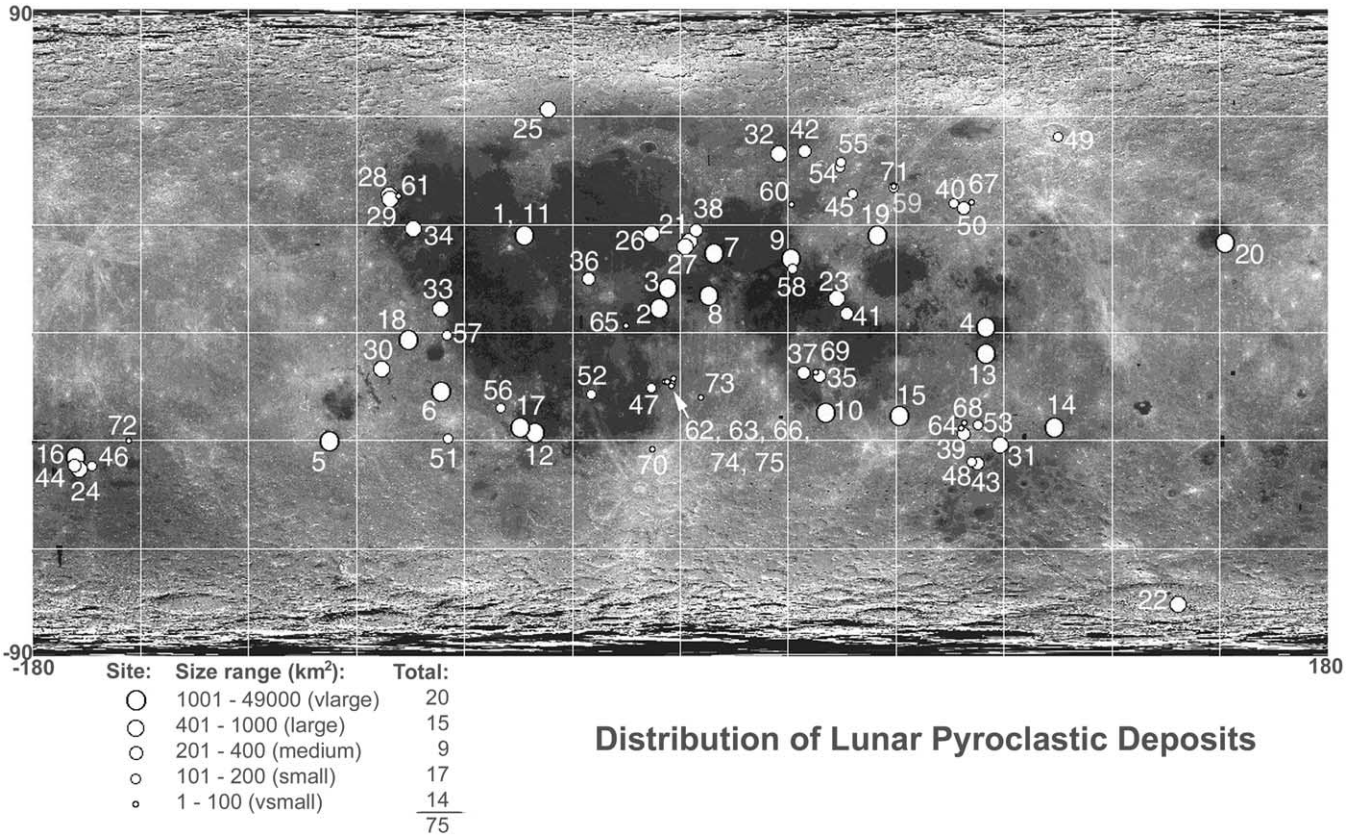

Fig. 2. Schematic map showing the spatial distribution of the 75 lunar pyroclastic deposits included in this analysis. The deposit locations are marked with white circles and sorted according to size: Very Large deposits (largest circles; 20 in number) are 1001 to 49,000 km^2 in size; Large deposits (second largest circles; 15 in number) are 401 to 1000 km^2 in size; Medium deposits (middle-sized circles; 9 in number) range from 201 to 400 km^2 in size; Small deposits (second smallest circles; 17 in number) are 101 to 200 km^2 in size; and Very Small deposits (smallest circles; 14 in number) are 1 to 100 km^2 in size. Numbers correspond to site entries in Table 1. Base image is the global 750-nm Clementine mosaic.

deposits are also observed in regions of thinned crust (~45 km), mostly in the South Pole/Aitken and Moscoviense basins. Formation of LPDs may have been favored near crater and basin margins by concentric extensional stresses occurring in some basins during relaxation following impact (e.g., Solomon et al., 1982).

II.C. Age

During the Apollo program, the extreme darkness of deposits at Taurus–Littrow along the southeastern margin of Mare Serenitatis was interpreted to mean that volcanism may have occurred recently at that site (e.g., Wilhelms and McCauley, 1971). Dark deposits such as those at Taurus–Littrow were also thought to be young because they had few superposed impact craters, but this was later realized to be due to abnormally rapid degradation of small craters in the unconsolidated pyroclastic material (Lucchitta and Sanchez, 1975). Later analyses of Apollo 17 samples from the Littrow valley revealed the presence of a small component of pyroclastic material (Howard et al., 1973) which is thought to dominate the Taurus–Littrow pyroclastic deposit that occurs ~30 km west of the Apollo 17 landing site (Adams et al., 1974). Age data revealed that this pyroclastic debris was emplaced at ~3.48 Ga (Tera and Wasserburg, 1976).

The experience of Apollo 17 at Taurus–Littrow indicated that low albedo could not be unequivocally associated with youth on the Moon, and it was soon realized that pyroclastic deposits probably mark the locations of source vents for earlier, presumably ancient volcanic eruptions (Head, 1974). This observation and the association of many LPDs with Imbrian-aged floor-fractured craters (e.g., Head and Wilson, 1979; Gaddis et al., 1998a, 1998b) or volcanic deposits (e.g., Whitford-Stark, 1990; Whitford-Stark and Head, 1980; Hiesinger et al., 2000) suggest that most of these deposits are of late Imbrian age, generally 3.2 to 3.7 Ga, corresponding to the age of the peak period of ancient lunar volcanism (e.g., Hiesinger et al., 2001). The existence of younger LPDs associated with episodes of more recent volcanism (extending to ~2.0 Ga; e.g., Hiesinger et al., 2001) cannot be ruled out, and at least one LPD near Taruntius crater has been suggested to be relatively young (possibly Eratosthenian in age; Spudis, 1989). Even if pyroclastic volcanism spanned the entire ~2-byr period of lunar volcanism, spectral observations of LPDs are expected to show that the surfaces of these deposits are spec-

trally mature (see Section III.A below), except where they have been disturbed by recent impacts.

II.D. Areal extent

For convenience, in previous studies (e.g., Gaddis et al., 1985), LPDs were divided into two major size-based classes: large or "regional" pyroclastic deposits (~20 in number) are of substantial spatial extent (>1000 km^2), whereas smaller, or "localized," deposits (~55 in number) are typically only several hundred km^2 in size. Often, the larger deposits do not have obvious vents; they may represent multiple deposits or their vents may have been covered by younger volcanic deposits. Many smaller deposits occur as dark haloes around semicircular or irregular depressions; these appear most likely to have been formed by single eruptive episodes. Examples include the endogenic "dark-halo craters" in the floor of the Nectarian crater Alphonsus (108 km dia.). Such deposits may occur on a crater floor at multiple sites (as in Alphonsus) or they may be relatively isolated (as in Schrödinger). Although these size classifications are somewhat subjective, LPD size is generally believed to be related to their mode of eruption and emplacement (see Section III.C. below). A detailed examination of the relationships between composition and size will thus permit refinement of our understanding of the influence of eruptive style on LPD composition.

For this analysis, the 75 pyroclastic deposits were arbitrarily grouped into five size classes, ranging from 3 to nearly 50,000 km^2 in areal extent (Table 1). Spatial extent or area in km^2 was estimated by identifying a low-albedo deposit in the Clementine 750-nm data and counting 100×100 m (or 0.01 km^2) pixels within the darkest albedo class. In some cases deposit boundaries are indistinct, and areal extents may include more than one deposit within a cluster. Twenty deposits, including those of Sinus Aestuum, Aristarchus plateau, and Oppenheimer NW, have been classified as Very Large, with areal extents from 1000 to nearly 50,000 km^2. Fifteen deposits (e.g., Oppenheimer S, J. Herschel) are described as Large, extending from 400 to less than 1000 km^2. Nine deposits (e.g., Fresnel, Oppenheimer SW) are classified as Medium and are 200 to less than 400 km^2 in size. Seventeen deposits, including those of Franklin and Oppenheimer SE, are Small, extending from 100 to less than 200 km^2. Finally, 14 deposits, such as those in Alphonsus and Apollo craters, are Very Small, or ~3 to less than 100 km^2.

II.E. Inferred eruption mechanisms

Dramatic variations in morphology, areal extent, and vent size and type have led scientists to infer fundamentally different eruption mechanisms for the large and small LPDs (e.g., Head and Wilson, 1979, 1992; Wilson and Head, 1981). Large pyroclastic deposits are thought to have been emplaced via more continuous, Hawaiian-style, fire-fountain eruptions (e.g., Wilson and Head, 1981), whereas smaller pyroclastic deposits were probably formed via intermittent, Vulcanian-style explosive eruptions (Head and Wilson, 1979).

More continuous lunar eruptions are likely to produce glass beads and crystalline or partially crystalline droplets (e.g., Heiken et al., 1974). With relatively low gravity and in the very dry, cold, near-vacuum environment at the lunar surface, an ascending magmatic column contains submillimeter-sized gas bubbles that explode upon reaching the surface (e.g., Head and Wilson, 1992). The resulting pyroclastic eruption plume contains submillimeter droplets of liquid magma propelled by and enveloped in a transient, volatile-enriched gas cloud (probably consisting of CO with S, Ag, Cd, Zn, and Br; Baedeker et al., 1974). More rapid cooling rates (on the order of 10 to 60°C/sec for the Apollo 17 orange glasses; Uhlmann et al., 1974) within such an erupting plume produce smaller quenched glass beads, whereas longer residence times (10 to 1000 times longer) within the cloud are likely to result in larger, compound droplets containing crystallites (Arndt et al., 1979, 1984).

These laboratory data raised the possibility that the relative amount of glass versus crystallized beads in a large pyroclastic deposit could be used to infer the eruption mechanism of that deposit. Glass-rich pyroclastic deposits are likely to have had relatively rapid cooling times within optically thin eruption plumes; deposits with abundant crystallized beads would have longer cooling times because of either their greater size and thickness or their eruption within a denser plume where temperatures remained higher for longer periods of time (e.g., Weitz et al., 1998). This possibility is explored further in Section III.B.3 below.

Eruption of small pyroclastic deposits has been modeled by Head and Wilson (1979). These authors suggested that substantial amounts of nonmagmatic materials (possibly basaltic caprock and wallrock of basaltic and/or highlands composition) were mixed with primary magmatic materials of basaltic composition during eruption of smaller pyroclastic deposits. Volumetric estimates of small pyroclastic deposits at Alphonsus crater indicated that some may consist of 50% to 100% of such nonmagmatic or nonjuvenile materials. Nonjuvenile materials are thought to have a larger average particle size than the relatively fine-grained juvenile pyroclastic materials produced by fragmentation of the magma (Head and Wilson, 1979).

II.F. Composition: previous work

Previous laboratory analyses and spectral characterization of samples from large LPDs and remote spectral observations of both large and small LPDs have contributed to our understanding of the origin of these deposits.

II.F.1. Sample data

Primary magmatic or juvenile components of the larger LPDs are thought to be the quenched glass and crystal-

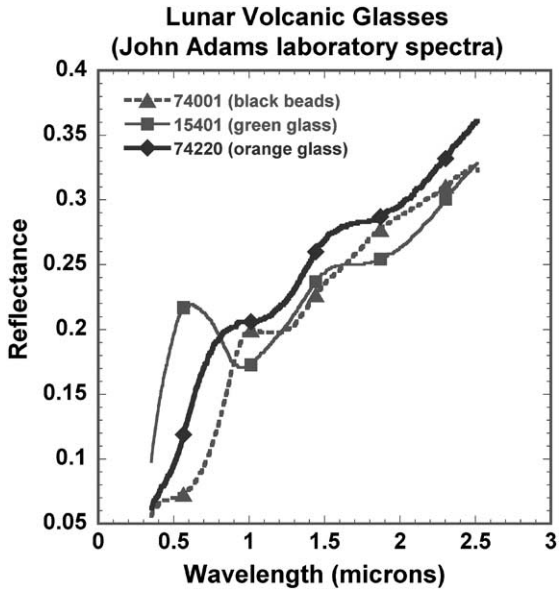

Fig. 3. Laboratory spectra of lunar pyroclastic spheres (after Pieters et al., 2000). Green glass from sample 15401 (square), orange glass from sample 74220 (diamonds), and black beads from sample 74001 (triangles) are shown.

lized volcanic beads resulting from gas-driven eruptions. Twenty-five varieties of volcanic glasses have been identified in lunar samples (Delano, 1986). Volcanic glass beads are recognized in lunar samples largely because they are uniform in texture and individually homogeneous in composition and have volatile-element-enriched surface coatings. Such coatings and the primitive compositions of glasses indicate that they come from deep within the Moon. Volcanic glasses have relatively high FeO (16.5 to 24.7 wt.%) and highly variable TiO_2 (0.26 to 16.4 wt.%) contents. Depending on composition, a variety of glass colors have been observed, including clear, yellow, orange, red, green, and brown glasses.

Laboratory spectral characteristics of the volcanic glasses at visible and near-infrared wavelengths (400 to 2500 nm, or 0.4 to 2.5 μm) show distinct differences from those of crystalline mare basalts (e.g., Pieters, 1993). Mare basalts may have absorption bands corresponding to the mafic minerals clinopyroxene (band center between 0.95 and 1.03 μm) and sometimes olivine (broad, multiple band centered at $\sim$1.1 μm), and lunar highlands units with mafic components can show spectral signatures of orthopyroxenes (or low-Ca pyroxenes; band center between 0.9 and 0.94 μm). By contrast, the amorphous, poorly ordered molecular structure of volcanic glasses of basaltic composition produces broad, less well-defined absorption bands centered near 1.0 and 2.0 μm (Fig. 3). Both the green glass from Apollo 15 and the orange glass from Apollo 17 have weak, broad, shallow bands centered near 1.0 and 1.8 μm that are due to Fe^{+2} in the glasses. However, the relatively high TiO_2 content ($\sim$9 wt.%) of the orange glass produces an absorption band with a "shoulder" that extends from the ultraviolet into the visible and near-infrared wavelengths; this UV/VIS slope causes the orange glasses to appear spectrally "red." This shoulder is absent in the green glass spectrum because it is low in TiO_2, but it is present in the spectrum for the Apollo 17 black volcanic beads (Fig. 3; Adams et al., 1974). Although the orange glasses and black beads have equally high FeO and TiO_2 contents, the black beads have distinctively flatter or low-contrast spectra, with a strong absorption band near 0.6 μm and weak or nonexistent bands at 1.0 and 2.0 μm. This low spectral contrast and the observed high UV/VIS ratio (or spectral "blueness") of the black bead deposits are due to the presence of sheaths of ilmenite crystals in a glass matrix (Pieters et al., 1974). Although olivine crystals are also present in the black beads, black bead spectra closely resemble those of the opaque mineral ilmenite (e.g., Adams et al., 1974; Pieters et al., 2000).

II.F.2. Remote observations

Earth-based telescopic observations and sample data suggest that many of the large lunar pyroclastic deposits, such as those at Taurus–Littrow, Rima Bode, Aristarchus, Sulpicius Gallus, and Sinus Aestuum have a major component of Fe^{+2}-bearing volcanic glass beads and/or chemically equivalent, black crystallized spheres (Pieters et al., 1973; Adams et al., 1974; Heiken et al., 1974; Lucchitta and Schmitt, 1974; Zisk et al., 1977; Gaddis et al., 1985; Lucey et al., 1986; Weitz et al., 1998). Remote observations indicate that several of these "black spot" deposits (notably those at Taurus–Littrow, Rima Bode, Sinus Aestuum, and Vaporum) contain significant amounts of black crystalline beads that result in their very low albedo and dominate their spectral response (Adams et al., 1974; Gaddis et al., 1985). Deposits such as those at Aristarchus plateau are thought to consist largely of quenched, iron-bearing volcanic glasses (Zisk et al., 1977; Lucey et al., 1986), and those at Sulpicius Gallus and elsewhere may consist of mixtures of black, crystallized beads and orange volcanic glasses (Lucchitta and Schmitt, 1974).

Earth-based spectral data for several smaller pyroclastic deposits indicate that a continuum of compositions exists for these deposits, extending from those with spectral properties that are comparable to mature highlands to those that are very similar to mature maria (e.g., Hawke et al., 1989a, 1989b; Gaddis et al., 2000). Only a few small LPDs, such as those at Alphonsus (Hawke et al., 1989b) and J. Herschel (McCord et al., 1981) craters, show spectral evidence of other components (such as olivine or glass) that might have been juvenile or derived from the primary magma. Remotely characterized compositions of the small pyroclastic deposits thus are related to the compositions of both the primary magma and the substrate through which the magma rose. Presumably the compositions of such low-volume eruptions are more likely to be influenced by mixing with local materials. While the influence of mixing with local highlands materials can be characterized remotely, it is not

possible to distinguish between intimately mixed juvenile and nonjuvenile mare basaltic components with remote spectral data alone. However, the presence of components such as olivine and glass in small pyroclastic deposits may be characterized with the 5-band Clementine UVVIS data.

Even with the help of sample data, it has typically been difficult to identify a clear genetic association between a particular pyroclastic deposit and a mare deposit. Although the formation ages of Apollo 17 orange glass (3.48 Ga) and Apollo 15 green glass (~3.3 Ga) are approximately consistent with the ages of nearby mare basalts, crystalline mare basalts with compositions comparable to the volcanic glasses have not been identified at any of the landing sites (e.g., Tera and Wasserburg, 1976; Delano, 1986; Lunar Sourcebook, 1991, Table A6.3, p. 205). Only the volcanic glasses at Apollo 17 were collected from a stratigraphic layer suggestive of a local volcanic origin. Green glasses were found in samples from the Apollo 15 site near Hadley Rille, but volcanic deposits with substantial green volcanic glass components have not been identified remotely. The spectral characteristics of LPDs in this region were thought to be more consistent with the presence of abundant yellow or brown glass components (Hawke et al., 1979), which were also sampled during Apollo 15.

III. Compositional analyses of lunar pyroclastic deposits

The 5-band Clementine UVVIS data at ~100 m/pixel (Eliason et al., 1999) were used to characterize the compositions of 75 large and small lunar pyroclastic deposits, and these were compared to compositions of major lunar maria and highland deposits (Gaddis et al., 2000; Gaddis et al., 2001; Petro et al., 2001; Staid, 2000; Staid and Pieters, 2000, 2001). Clementine UVVIS data were obtained at wavelengths of 415, 750, 900, 950, and 1000 nm. These data are used to (1) determine the compositional diversity of lunar pyroclastic deposits, (2) identify and characterize juvenile components where possible, (3) compare the compositions of large and small pyroclastic deposits to evaluate the influence of size on the inferred eruption mechanisms, and (4) evaluate the compositional relationships, if any, between lunar pyroclastic and mare deposits.

As observed in the Clementine UVVIS spectra (Gaddis et al., 2000, and this analysis), most LPDs exhibit the subdued mafic absorption bands typical of those of mature mare or highlands soils (Fig. 4). The presence of a broad absorption band centered longward of 1.0 μm that might be due to ferrous iron in volcanic glass or olivine in some of these mature LPDs (e.g., Aristarchus, J. Herschel) is not strongly evident in the Clementine UVVIS spectra (Fig. 4). Typical mature LPDs do not have strong mafic absorption bands such as that of the fresh materials in the wall of the mare crater Jansen (13.5°N, 28.7°E; 23 km dia.), where a clinopyroxene band is observed at ~0.95 μm. Most of the

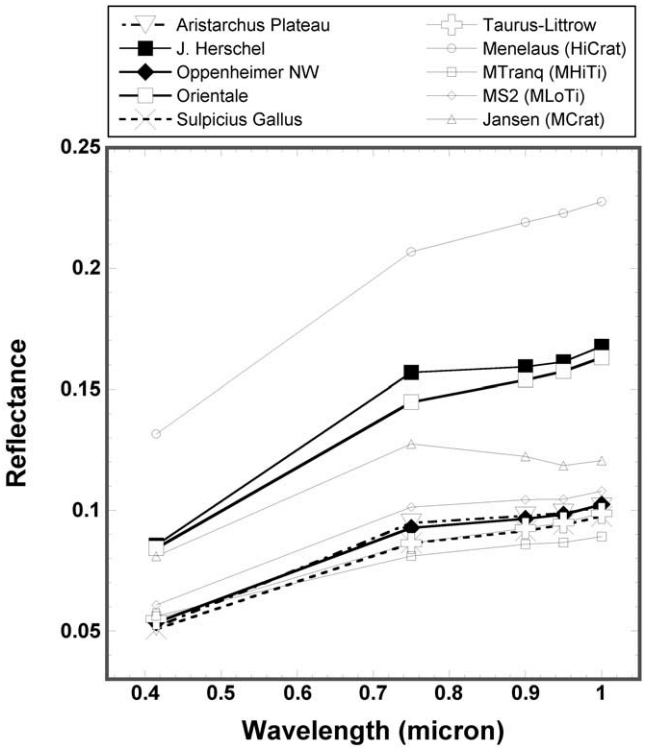

Fig. 4. Clementine UVVIS spectra for pyroclastic deposits at Aristarchus plateau, J. Herschel, Oppenheimer crater, Orientale, Sulpicius Gallus, and Taurus–Littrow. For comparison, spectra from Menelaus (a highlands crater; 16.3°N, 16.0°E), Mare Tranquillitatis ("Mtranq", a high-titanium mare deposit), Mare Serenitatis ("MS2", a low-titanium mare deposit), and Jansen (a mare crater; 13.5°N, 28.7°E) are also shown.

LPDs have reflectances at 750 nm (or "albedos") that are much lower than that of fresh highlands (Menelaus crater) and are bracketed by typical high-titanium (Mare Tranquillitatis or Mtranq, Fig. 4) and low-titanium (Mare Serenitatis-2 or MS2) mature maria. However, the LPDs at J. Herschel and Orientale have higher average albedos that are more typical of mature highlands. Although the relatively high albedo of the Orientale deposit may be due to its thinness (Head et al., 2002), the relatively flat slope between 0.75 and 0.90 μm in the spectrum of J. Herschel may indicate the presence of a brighter mafic component (possibly olivine or iron-bearing glass) that has broadened the absorption band and increased the albedo of the pyroclastic deposits of J. Herschel (McCord et al., 1981). To examine the compositions of LPDs in more detail, Clementine albedo and color ratio data are addressed below.

III.A. Parameterization of LPD composition and comparison to maria and highlands

To characterize the compositions of LPDs and to compare them to those of lunar maria and highlands, data on reflectance at 750 nm (or "albedo") and two color ratios were examined (Figs. 7, 8, 9 below). Albedo at 750 nm is a first-order indicator of differences in brightness due to vari-

ations in soil mineralogy and chemistry, maturity, particle size, and viewing geometry effects. As is the case for mature mare soils, primary compositional differences among the LPDs include relative titanium content (e.g., Johnson et al., 1991) and relative mafic content and composition (e.g., Pieters et al., 1993; Pieters, 1993). The relative titanium content of mature basaltic soils is commonly estimated by the slope of the line between reflectances at 415 and 750 nm (or the "visible slope"), or equivalently by the 415/750-nm (or UV/VIS) ratio (e.g., Charette et al., 1974; Johnson et al., 1991). Deposits with high 415/750 values have higher titanium contents and have historically been called "blue"; deposits with low values have lower titanium contents and are "red" (e.g., Wilhelms, 1987). The mafic content is related to the 1.0-μm or mafic band strength, or the ratio of 950/750 nm reflectances. Deposits with low 950/750 values generally have deeper 1.0-μm bands and stronger mafic spectral signatures, and those with high 950/750 values have shallower 1.0-μm bands and weaker mafic signatures. In addition to providing effective compositional discrimination among LPDs and mare deposits, these two spectral ratio parameters (as measures of relative reflectance) serve to minimize small residual photometric variations due to viewing geometry effects.

Before using Clementine albedo and color ratio data for characterizing LPD compositions (e.g., Gaddis et al., 2000), at least one major caveat to their usage for this purpose must be presented. These tools do not completely characterize the composition of high-titanium LPDs with either substantial crystalline (particularly opaque mineral) components or orange glasses. The best example of such a deposit is that of Taurus–Littrow, but several other deposits, including Rima Bode, Sinus Aestuum, Vaporum, and Sulpicius Gallus, are also believed to have substantial crystallized bead components (e.g., Pieters et al., 1974; Gaddis et al., 1985). Although at the Apollo 17 site the ilmenite-rich "black beads" are compositionally equivalent to the high-FeO and high-TiO_2 orange glasses, the spectral behaviors of these two components are markedly different. As noted earlier, the TiO_2 in the Apollo 17 orange glasses produces an absorption shoulder extending from shorter (UV) wavelengths into the visible, while the FeO produces absorption bands near $\sim$1.0 and 2.0 μm. The orange glasses thus have a low 415/750 nm or "red" UV/VIS ratios. For the black beads, crystallinity has decreased the albedo, reduced the spectral contrast, and weakened the mafic band for these deposits. The prominent ilmenite absorption band at 0.6 μm in the black-bead LPDs produces a high 415/750 nm or a "blue" UV/VIS ratio; as a result, deposits rich in these black beads exhibit different (higher) UV/VIS values despite having similar TiO_2 contents to the orange glasses. Although comparisons among these LPDs and between these and other LPDs are valid, the Clementine compositional data are not strict indicators of either iron or titanium content for these Very Large, crystalline bead or orange-glass-enriched LPDs. As shown below, these deposits are unique among lunar deposits and are not representative of the majority of LPDs.

III.A.1. Mafic band strength (950/750 nm) versus albedo (750 nm)

In Fig. 5, mafic band strength (950/750 nm) versus albedo are compared for 75 LPDs and for a selection of representative mare and highland terrains. Data for the lunar maria (open crosses, italic labels, darker gray polygonal region) are average values for uncontaminated, mature mare soils from Staid (2000). Major mare units are labeled after the compositional classification of Pieters (1978) in which the first letter refers to the slope of the UV/VIS ratio, the second to albedo, and the third and fourth letters to the depths of the 1- and 2-μm bands, respectively. Highlands data ("X" symbols, lighter gray polygonal region) are generally for mature soils (weaker mafic bands), but two fresher deposits (with stronger mafic bands, lower right) are included for comparison. The polygonal outlines for the maria and highlands spectral regions are approximate; both regions could overlap in the middle and could extend further up toward weaker band strengths if less typical soils were included. Less mature soils of all types are found toward the lower right in Fig. 5. Within the mare region, more iron and titanium-rich soils have lower albedos and a range of mafic band strengths. However, most high-titanium, high-iron maria are observed on the left side of the mare region, and lower titanium soils are found on the right side largely due to differences in their 750 nm albedos.

The LPD values in Fig. 5 (filled symbols, five size classes) are generally broadly distributed across the mare region and are observed on the lower albedo (left) side of the highland region. Only one cluster of LPD compositions is observed (at upper left) and it includes the five unusual and apparently distinctive Very Large "black bead" deposits (Sinus Aestuum, Taurus–Littrow, Vaporum, Rima Bode, and Sulpicius Gallus) noted above.

The values of other Very Large LPDs in Fig. 5 are distributed across the maria region and some (e.g., Orientale, Smythii) extend toward higher albedos and have weaker mafic bands than typical maria. Large LPDs are equally broadly distributed within the maria region; most have moderate mafic bands and a range of albedos. Two Large LPDs, J. Herschel and Schrödinger, have unusually strong mafic bands and relatively high albedos. Medium LPDs are commonly observed in the upper portion of the maria region, with moderate to weak mafic bands and a range of albedos. Two Medium LPDs (Abel B and Gauss S, both unlabeled on Fig. 5) have albedos sufficiently high to fall well within the highlands region. Small LPDs are widely distributed within the maria region, with a broad range of mafic band strengths and albedos. Several Small LPDs fall within the highlands region, with relatively high albedos and moderate to weak mafic bands. Finally, the Very Small LPDs also are observed within both the maria and highlands regions; most have moderate to high albedos

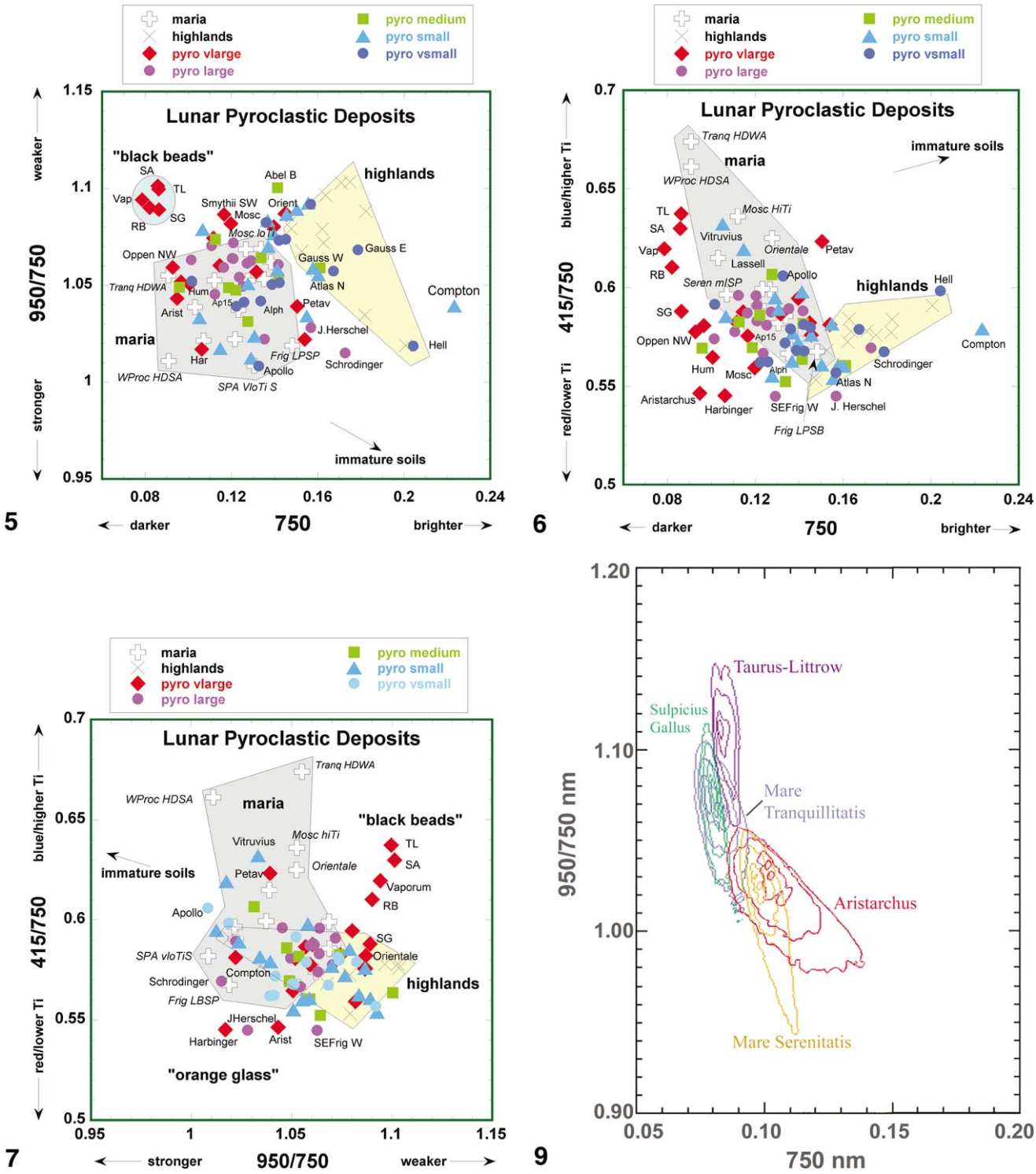

Fig. 5. Clementine color ratio data at 950/750 nm versus albedo at 750 nm for 75 pyroclastic deposits grouped into 5 size classes. For comparison, data are also presented for 14 lunar mare soils (gray region, after Staid, 2000) and for 10 highland soils of varying maturity (yellow region).

Fig. 6. Clementine color ratio data at 415/750 nm versus albedo at 750 nm for 75 pyroclastic deposits grouped into 5 size classes. For comparison, data are also presented for 14 lunar mare soils (gray region, after Staid, 2000) and for 10 highland soils of varying maturity (yellow region).

Fig. 7. Clementine color ratio data at 415/750 nm versus 950/750 nm for 75 pyroclastic deposits grouped into 5 size classes. For comparison, data are also presented for 14 lunar mare soils (gray region; after Staid, 2000) and for 10 highland soils of varying maturity (yellow region).

Fig. 9. Scatterplot of pixel brightness variation for the 950/750 color ratio versus albedo at 750 nm. Data for pyroclastic deposits at Taurus–Littrow, Sulpicius Gallus, and Aristarchus plateau are overlaid onto data for mare deposits at Tranquillitatis and Serenitatis. For each region, more mature materials are found at the top end of the scatterplot. Contours mark “freshness” densities at 1%, 10%, 50%, and 80% of surface materials.

and show a wide range of mafic band strengths. Several Small and Very Small LPDs (e.g., Gauss E and W, Atlas N, Hell, Compton) have albedos comparable to typical highlands and thus lie well within the highlands region. The Small LPD at Compton shows an unusually high albedo that exceeds the brightness of typical highlands.

The majority of LPDs fall within the maria region in Fig. 5. The larger LPDs (most members of the Very Large, Large, and Medium classes) generally match the range of mafic band strengths and albedos observed for typical maria. The smaller LPDs (Small and Very Small) have the widest range of albedos and mafic band strengths, with many observed in an overlap zone between maria and highlands. LPDs have a wide range of albedos and many are not especially dark. Two mare deposits (WProc HDSA, Tranq HDWA) are darker than most of the LPDs. With the exception of the five Very Large "black bead" LPDs, strong clusters are not observed among the LPDs on the basis of albedo, mafic band strength, or size. There is no obvious correlation between albedo and mafic band strength for either the mare soils or the majority of the LPDs.

These data indicate that the compositions of most LPDs are comparable to those of lunar mare soils. This relationship is true for LPDs regardless of inferred eruption mechanism, including both several Very Large deposits presumably emplaced by fire-fountaining (Aristarchus, Humorum) and many LPDs which are clearly endogenic or "dark halo" pyroclastic deposits (e.g., Alphonsus, Apollo). LPDs which are thought to be glass-rich, such as Aristarchus, Harbinger, and Apollo 15, fall well within the maria region in average composition. The J. Herschel LPD, thought to have a substantial olivine or possibly iron-bearing glass component (McCord et al., 1981; Hawke et al., 1989a, 1989b), plots near the Frigoris low-titanium mare deposit. LPD compositions enriched in iron-bearing glass and/or olivine (J. Herschel, Aristarchus) cannot be distinguished from high-calcium pyroxene compositions typical of lunar maria when viewed in terms of albedo and mafic band depths.

The effects of mixing with highland compositions are clear for many of the smaller LPDs. Approximately 20% of the LPDs, mostly smaller deposits, overlap with mature highlands in albedo and mafic band strength. This similarity to highlands compositions may be due to primary compositional effects (incorporation of highlands substrate material during eruption; Hawke et al., 1989a, 1989b) or to secondary contamination effects (e.g., superposition of younger crater rays or vertical mixing). Clear examples of the latter effects are observed for Compton, Gauss, Oppenheimer SE, and perhaps Schrödinger.

III.A.2. Visible slope (415/750 nm) versus albedo (750 nm)

The maria and highlands regions overlap at moderate albedos and low 415/750 nm or UV/VIS (Fig. 6). Typical highlands have relatively high albedos and low 415/750 values (i.e., are relatively "red"), whereas the maria have lower average albedos and a much broader range of 415/750 values. Two of the maria, Tranquillitatis HDWA and Western Procellarum HDSA, are very "blue" and have been inferred to have high titanium contents (>8 wt. %; Johnson et al., 1991; Giguere et al., 2000). Recent work on the Western Procellarum basalts has suggested that the estimated TiO_2 content of that deposit should be revised to the moderately high range (~6 to 8 wt. %; Gillis and Jolliff, 2001a, 2001b, 2001c; Gillis et al., 2001). Note, however, that both Tranquillitatis HDWA and Western Procellarum HDSA have higher inferred TiO_2 contents than all other lunar basalts. The low-titanium mare deposit of Frigoris (LBSP), with higher average albedo and low or "red" 415/750 values, marks the opposite extreme in composition among the maria in Fig. 6.

One apparent trend in Fig. 6 is worthy of note. Several of the Very Large LPDs, including the "black bead" deposits of Taurus–Littrow, Sinus Aestuum, Vaporum, Rima Bode, and perhaps Sulpicius Gallus, are lower in albedo than typical maria. These very dark LPDs are the "blue" members of a nearly linear trend of decreasing 415/750 values that includes several Very Large LPDs that are slightly brighter and spectrally "red." The Taurus–Littrow, Sinus Aestuum, Vaporum, and Rima Bode LPDs are all very "blue" and are known or inferred to have a significant component of high-titanium materials (in the form of ilmenite-rich black beads). Deposits such as those at Sulpicius Gallus have intermediate UV/VIS ratio values perhaps due to fewer opaque minerals. Oppenheimer NA, Humorum, Aristarchus, and Harbinger LPDs have low 415/750 values and may have lower titanium contents. Although it is intriguing to speculate that this trend is related directly to variations in titanium content among these Very Large LPDs, it more likely represents a complex combination of the degree of crystallinity (i.e., ilmenite content) of the high-iron, high-titanium LPDs (Taurus–Littrow, Sinus Aestuum, Vaporum, Rima Bode, and possibly Sulpicius Gallus) and possibly variations in titanium content of the iron-rich glassy deposits (Oppenheimer NW, Humorum, Aristarchus, Harbinger).

Most of the other LPDs, regardless of size, overlap with the moderate- to low-titanium mare basalts. A few LPDs (~10) fall outside the maria field toward lower albedos and redder colors, and an equal number have higher albedos comparable to typical highlands. For these "mare like" LPDS, there is a weak trend of decreasing albedo and increasing titanium content, similar to but weaker than that observed for the mare basalts. A few LPDs, such as the Large deposits at J. Herschel and SE of Frigoris W, have relatively red UV/VIS properties (and inferred low titanium contents), whereas Small deposits such as Vitruvius, Lassell, and Apollo are bluer and have apparently higher titanium contents. A slight correlation exists between size and albedo, with many of the largest LPDs having lower albedos than most of the smaller deposits.

III.A.3. Visible slope (415/750 nm) versus mafic band strength (950/750 nm)

Albedo is not a factor in this parameterization, so there is greater overlap between the maria and highlands fields (Fig. 7). Most of the LPDs, regardless of size, fall within the lower 415/750 ("redder") portion of the mature maria field where there is substantial overlap with the highlands field, and several LPDs extend into the highlands-only region. Whereas most LPDs have lower 415/750 values and may have relatively low TiO_2 contents, they have a range of mafic band strengths spanning that of both typical mature maria and highlands. For example, several LPDs (Aristarchus, Harbinger, and J. Herschel) have lower 415/750 values than typical maria and may have substantial low-titanium glass and/or olivine components.

For most LPDs, no strong correlation exists between mafic band strength and UV/VIS ratio (Fig. 7). The "black bead" deposits at upper right (Taurus–Littrow, Sinus Aestuum, Vaporum, and Rima Bode) again form a distinctive cluster, with high or blue 415/750 values and very weak mafic bands. If the "black bead" deposits are compared to many other Very Large LPDs, a cross-cutting, upper-right to lower-left trend suggests that deposits with higher TiO_2 contents have weaker mafic bands and those with possibly lower TiO_2 contents have stronger mafic bands. This is in contrast to the nearly vertical trend for the mature maria, in which mafic band strength is relatively independent of TiO_2 content. However, it has been suggested that some mare units have relatively low "1-μm" band strengths because of a reduction in spectral contrast due to presence of abundant dark TiO_2-rich material (McCord et al., 1981). Indeed, if the Western Procellarum HDSA deposit is removed from consideration, then the maria may actually show two parallel cross-cutting trends extending from higher 415/750 and weaker mafic bands to lower 415/750 values and stronger mafic band strengths.

The cross-cutting trend among the LPDs, extending from Taurus–Littrow at the top right (very weak mafic band, very blue, high titanium content) through Sulpicius Gallus, Orientale, and Humorum to Aristarchus and Harbinger (red, low UV/VIS, possibly lower titanium content, stronger mafic band) at the lower left, has also been proposed as a "mixing line" between the large pyroclastic deposits with predominantly crystallized black beads at the top to those with mostly iron-bearing glass beads at bottom (Weitz et al., 1998). This hypothetical mixing relationship, a measure of the "glassiness" of a pyroclastic deposit with implications for its mechanism and duration of eruption, assumes that titanium contents for the LPDs along this trend are equal. Two aspects of this possibility warrant further discussion. First, it is known that these 415/750 nm or UV/VIS color ratio and 950/750 nm or mafic band depth data cannot be interpreted strictly in terms of iron and especially titanium content for the "black bead" or orange glass deposits, meaning that their placement with respect to other deposits on Fig. 7 must be considered relative and not absolute. Second, it is clear in Figs. 6 and 7 that the LPDs at Aristarchus, Harbinger, and J. Herschel have lower UV/VIS ratios than most other LPDs. J. Herschel is thought to have a substantial olivine and possibly a glass component with low titanium content (McCord et al., 1981, Hawke et al., 1989a, 1989b). LPDs at Aristarchus and Harbinger were once thought to consist largely of iron-bearing orange glass and possibly black beads comparable to those found at the Apollo 17 site (Zisk et al., 1977). More recently, Lucey et al. (1986) suggested that the very strong, broad 1.0-μm mafic band observed in Earth-based spectra for the LPDs at Aristarchus was due to a substantial component of iron-bearing glass.

Data in this paper support the argument that LPDs such as Aristarchus and Harbinger are very glass-rich, and it is likely that these spectrally "red" LPDs have a substantial component of an iron-bearing glass with a different composition from the LPD at Taurus–Littrow. Additional evidence in support of this possibility comes from comparison of spectra for a fresh Apollo 17 orange glass and the mature LPD at Aristarchus (Fig. 8); it is apparent that the 1.0-μm mafic band depth for the Apollo 17 orange glass is less than that of the Aristarchus LPD. Because band depths decrease in strength with increasing maturity, a strong mafic band such as that observed at Aristarchus cannot be produced by weathering of a deposit strongly enriched in orange glass with a weaker mafic band.

The Aristarchus LPD may consist of an iron-bearing orange glass with a lower titanium content than the high-titanium contents (10 to 16 wt. %; Delano, 1986) typically cited for orange glasses at Apollo 17. For example, Aristarchus iron-bearing glasses may resemble the lower-titanium orange glasses from Apollo 17, with TiO_2 values of $\sim$7 wt. %. If this is the case, then variations in glassiness and crystallinity are probably not the sole source of the cross-cutting trend for UV/VIS and mafic band depth for all of the Very Large deposits. It may be that differences in crystallinity for the mixtures of high-titanium orange glasses and black beads at Taurus–Littrow produce the observed variations in spectral ratio for deposits at this site and at Sinus Aestuum, Rima Bode, Vaporum, and possibly Sulpicius Gallus. If the LPDs at Aristarchus, Harbinger, and possibly Humorum consist of iron-rich glasses unlike those at Taurus–Littrow, then intrinsic variation in titanium content, perhaps along with degree of crystallinity, may produce the observed spectral ratios. Resolution of this possibility awaits independent information on titanium contents among the LPDs, such as might be derived from Lunar Prospector data (e.g., Lawrence et al., 1998; Elphic et al., 1998; Prettyman et al., 2002).

III.B. Effects of maturity

Because Clementine spectral data for many of the mature LPDs show weak mafic absorption bands, the question arises as to how well the Clementine data are representing true pyroclastic deposit compositions, particularly the juvenile components such as volcanic glasses. This issue has

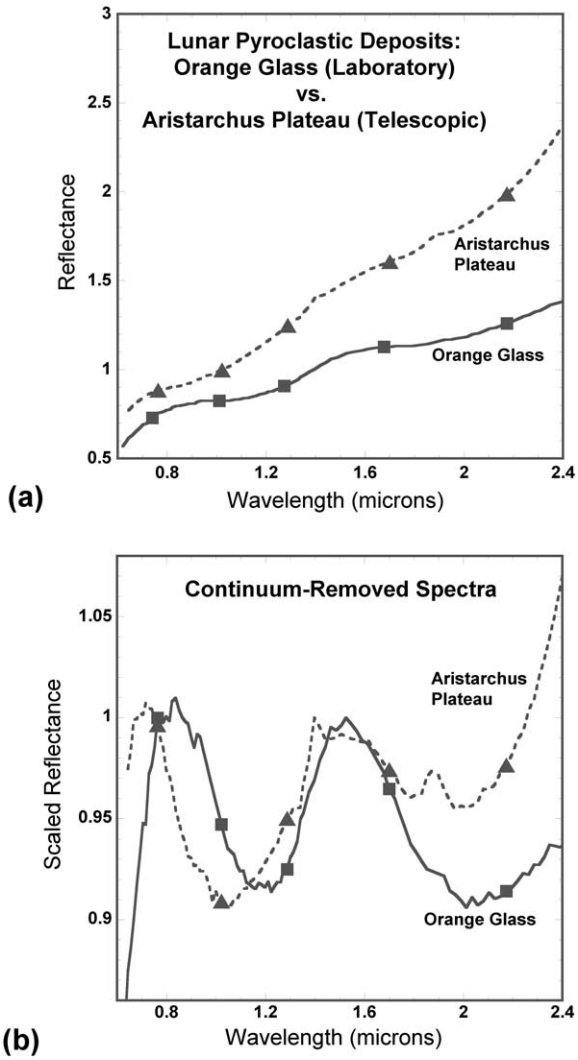

Fig. 8. Spectra for orange glass (Apollo 17 sample 74220, from J. Adams collection) and the mature LPD at Aristarchus plateau. The laboratory spectrum for orange glass has been resampled to a lower spectral resolution and scaled in reflectance for comparison with the telescopic spectrum for Aristarchus plateau (see Fig. 3 for true orange glass spectrum). Both spectra are from the NASA RELAB collection at Brown University. (a) Reflectance spectra. (b) Spectra from which a linear continuum has been removed near 0.75 to 1.5 μm to enhance and compare the mafic band depth at 1.0 μm. Note that the 2.0 μm bands are not correctly portrayed in this figure because the continuum does not extend to those longer wavelengths.

been addressed for several lunar maria by comparing spectral characteristics of relatively unaltered surfaces in ejected materials of fresh craters small enough to have penetrated into but not through the deposits with spectra of associated mature soils (e.g., Staid, 2000). Maturity effects are not as readily characterized among the LPDs because their deposit sizes are small, they are relatively thin (e.g., much less than 10 m for Orientale (Head et al., 2002) and 50–100 m for Aristarchus plateau (Zisk et al., 1977)), and they have infrequent small craters that might have impacted into them but not penetrated through them. However, variations in mafic band depth attributable to maturity can be observed near small craters in several of the Very Large pyroclastic deposits such as those at Taurus–Littrow, Vaporum, Sulpicius Gallus, and Aristarchus.

Weathering or maturity trends for several LPDs are characterized here by comparing variations in mafic band strength (950/750 nm ratio) versus albedo (at 750 nm) for materials with a full range of maturities from Mare Tranquillitatis (a high-titanium, high-iron basalt), central Mare Serenitatis (a low-titanium, high-iron basalt), and pyroclastic deposits at Taurus–Littrow, Sulpicius Gallus, and Aristarchus (Fig. 9). Note that the presence of higher-albedo highland materials in these isolated units is easily detected as a right-trending bulge or "wing" in such scatterplots; such pixels have been eliminated from this analysis. Within each data cloud, the most mature materials are at the upper left; with decreasing maturity there is an increase in both albedo and mafic band strength.

Although all materials in Fig. 9 exhibit relatively low albedos, they have widely varying mafic band strengths. Mature pyroclastic materials at Taurus–Littrow have distinctively low albedos and the weakest mafic band, and fresh mafic materials from Mare Serenitatis are brighter and have the strongest mafic band. Less mature Taurus–Littrow material and both mature and less mature materials from the LPD at Sulpicius Gallus are very dark and have slightly stronger (but still relatively weak) mafic bands that are similar to those of the high-titanium Tranquilitatis mare deposit. The Sulpicius Gallus LPD is generally intermediate in band strength between Taurus–Littrow and Aristarchus LPDs. The Aristarchus Plateau LPD is more comparable in albedo and mafic band strength to mature Mare Serenitatis low-titanium basalt.

The maturity trends in Fig. 9 are consistent with previous results indicating the presence of opaque, high-titanium, crystallized pyroclastic beads at both Taurus–Littrow and Sulpicius Gallus, and with an iron-bearing glassy (but probably not high-titanium) mafic component at Aristarchus Plateau. The spectral signature of the Taurus–Littrow LPD is dominated by the black beads (e.g., Pieters et al., 1974), regardless of maturity. The stronger mafic band strength of less mature materials at Sulpicius Gallus may support previous interpretations of spectral data indicating that the Sulpicius Gallus LPD consists of a mixture of both black beads and orange glasses (e.g., Gaddis et al., 1985; Weitz et al., 1998). Inflight astronaut observations of the visibly reddish or brown LPD at Sulpicius Gallus suggested that it has a higher abundance of orange glasses than the LPD at Taurus–Littrow (Lucchitta and Schmitt, 1974). However, the stronger mafic band and higher average albedo of the Aristarchus Plateau LPD indicate that it has a large component of iron-bearing glass (e.g., Lucey et al., 1986); our data suggest that the Aristarchus deposit has a relatively low to moderate titanium content. Thus, compositional distinctions among the LPDs can be recognized across maturity states. Maturity variations are present within and between these deposits, but they are secondary to compositional variations

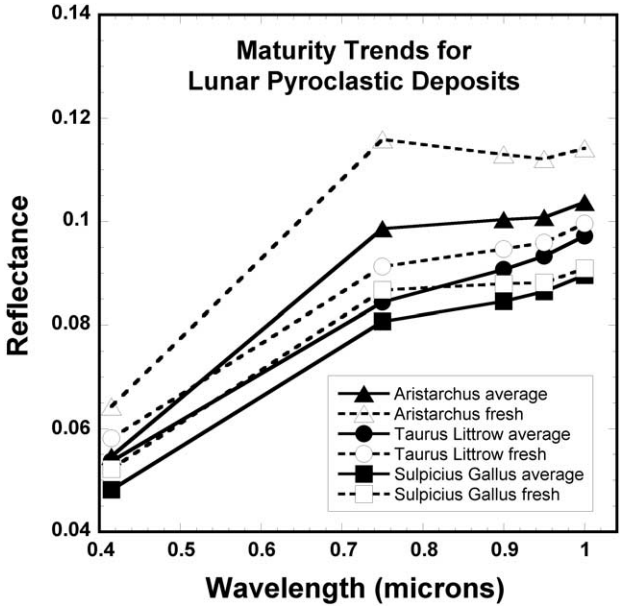

Fig. 10. Clementine UVVIS spectra for mature and fresh materials (the least mature 0.5%) for pyroclastic deposits at Aristarchus plateau (triangles), Taurus–Littrow (circles), and Sulpicius Gallus (squares).

because only small fractions of the deposit surfaces are immature.

Clementine UVVIS spectra for the freshest and most mature fractions of LPDs at Aristarchus, Taurus–Littrow, and Sulpicius Gallus (Fig. 10) show similar maturity trends. Spectra for mature fractions of both Taurus–Littrow and Sulpicius Gallus LPDs have low albedos and very weak mafic absorption bands. By contrast, the freshest materials have higher albedos and stronger mafic absorption bands. The difference in mafic band depth between the mature and fresh materials at Sulpicius Gallus is greater than that of Taurus–Littrow; these data are consistent with the presence of a higher abundance of orange glasses in the mixture of orange glasses and black beads at Sulpicius Gallus. For the higher albedo LPD at Aristarchus (Fig. 10), the contrast is even greater between mature and fresh fractions. Though the mafic band is evident in the mature fraction, a clear, broad mafic absorption band is attributable to iron-bearing volcanic glasses in the fresher materials at Aristarchus.

Although these spectral differences between fresh and mature LPD materials provide data on the compositions of juvenile pyroclastic materials, they do not change the overall compositional relationships observable in the Clementine data for mature LPDs. It is evident that the Clementine UVVIS data for LPDs are most strongly influenced by compositional and not maturity variations and thus they provide meaningful information on LPD compositions.

IV. Discussion

Analyses of Clementine UVVIS data indicate that overall compositions of most LPDs, particularly the Medium, Small, and Very Small deposits, closely resemble those of average mare soils with low to moderate TiO_2 contents. These data suggest that the majority of LPDs have juvenile magmatic components that may consist of fragmented basalts, with substantial components of iron-bearing mafic minerals (pyroxenes, olivine, occasionally ilmenite) and smaller amounts (if any) of iron-bearing volcanic glass spheres in either quenched or crystallized form. These results confirm those of previous investigations (e.g., Hawke et al., 1989b; Blewett and Hawke, 2001) in which a class of small pyroclastic deposit with a large mare basalt component was identified. For such deposits, Hawke et al. (1989b) proposed an origin by vulcanian eruption in which the proportion of entrained, ejected basaltic plug rock is high compared to that of wall rock and juvenile materials. Many of the LPDs in this analysis may have had similar origins.

In general, results of this analysis support previous research suggesting that size or areal extent of an LPD can be related to an inferred eruption style, with larger deposits formed by more continuous fire-fountaining from larger vents and smaller deposits by intermittently explosive vulcanian eruptions from smaller vents (e.g., Wilson and Head, 1981; Head and Wilson, 1979). For example, Very Large LPDs at Taurus–Littrow, Rima Bode, and Aristarchus Plateau include those typically recognized as having been produced by fire-fountain from larger vents or rilles. Most of the Large, Medium, Small, and Very Small LPDs are observed as relatively isolated deposits in the highlands or in crater floors near younger mare deposits (e.g., Oppenheimer SW, J. Herschel, Lavoisier H, Apollo), environments typical of deposits formed by vulcanian eruptions. However, the Very Large LPD at Oppenheimer NW occurs in a farside floor-fractured crater. Although it is $\sim$1500 km^2 in size, the Oppenheimer NW deposit has been described by Head et al. (2001) as the product of a vulcanian eruption comparable to that inferred for endogenic deposits at Alphonsus. Clementine UVVIS spectral analyses of the Oppenheimer LPDs of all sizes (this work, and Petro et al., 2001) indicate that they have comparable albedos and mafic band strengths but lower UV/VIS ratios (i.e., they are "redder") than most lunar maria, they show limited compositional diversity, and they resemble several Very Large LPDs in overall color, including Aristarchus, Humorum, and Dopplemayer. If, like Aristarchus, the Oppenheimer NW LPD has a substantial component of volcanic glass, then it would be unique among LPDs formed by vulcanian eruption in having a recognizable major glass component.

Several LPDs (notably Schrödinger, Compton, and Orientale) closely resemble mature lunar highlands in overall composition, but different mechanisms may have produced these spectral signatures. For the relatively high-albedo deposits at Schrodinger, entrained feldspathic country rock may be the volumetrically dominant component. At Compton, mixing with highlands material has an obvious influence on composition. Finally, the LPD at Orientale may resemble highlands because it is a very thin (estimated

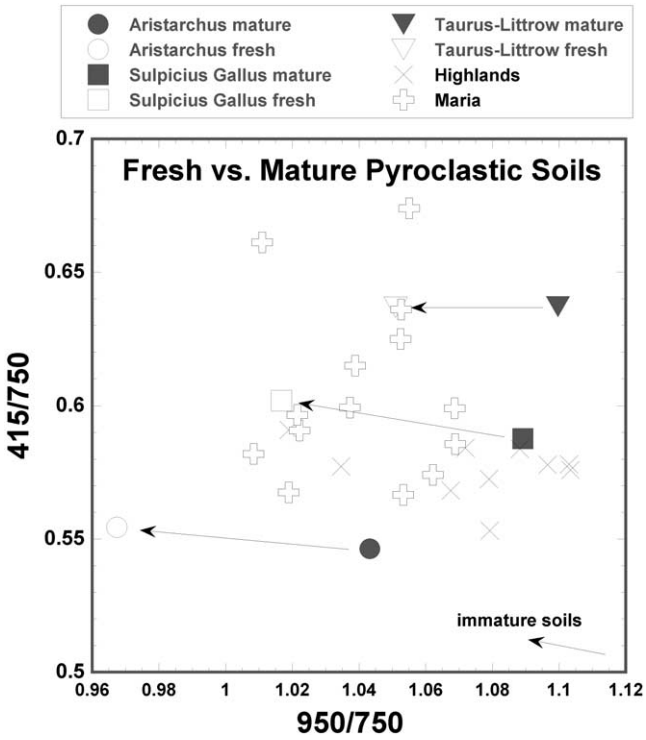

Fig. 11. Clementine color ratio data at 415/750 versus 950/750 for pyroclastic deposits at Taurus–Littrow, Sulpicius Gallus, and Aristarchus. Solid symbols mark the color ratio values for mature soils, and open symbols are for immature (freshest 1%) soils. For comparison, data are also presented for 14 lunar mare soils (after Staid, 2000) and for 10 highlands soils of varying maturity.

thickness much less than 10 m, Head et al., 2002) deposit superimposed on highlands terrain.

The majority of LPDs can be considered separately from the Very Large crystallized "black bead" deposits, which remain compositionally distinctive. The high FeO contents of the "black bead" deposits are not accurately demonstrated by their weak mafic absorption bands in the Clementine UVVIS data. Other Very Large or Large deposits (Aristarchus, Harbinger, Humorum) are thought to have substantial iron-bearing volcanic glass components, and these are distinctively "red" with likely lower titanium contents, moderate to low albedos, and moderately strong 1-μm mafic absorption bands. The glass-rich LPD at Aristarchus remains distinctive even in its immature or "fresh" state, whereas fresh materials in the "black bead" deposit at Taurus–Littrow and the possibly mixed glass/crystallized bead deposit at Sulpicius Gallus resemble mature maria in the color ratio plot shown in Fig. 11.

Future work may help to clarify further the compositions of lunar pyroclastic deposits, especially the chemistry, physical characteristics, and relative volumetric significance of the primary or juvenile magmatic component. For example, the Clementine UVVIS data provide information on the 1-μm absorption feature of volcanic glass; data for the long-wavelength portion of the 1-μm band and the entire 2-μm band await release of calibrated Clementine near-infrared (NIR) camera data. With combined UVVIS and NIR data, we may be able to distinguish between the presence of olivine and iron-bearing glass and to characterize the relative importance of these possible magmatic components. Also, analyses of higher-spatial-resolution data on TiO_2 contents from Lunar Prospector data (e.g., Prettyman et al., 2002) may help to constrain the titanium contents of some of the larger LPDs, perhaps allowing comparison of one of the high-titanium "black bead" deposits such as Rima Bode with that of Aristarchus to assess the titanium content of the iron-bearing glass in the latter region.

V. Conclusions

The following conclusions are supported by our compositional analyses of 75 lunar pyroclastic deposits (LPDs) with Clementine UVVIS data:

1. LPDs are widely distributed across the Moon (Fig. 2), are generally observed in the highlands near mare deposits and/or in the floors of craters, and are often found in association with fractures, irregular depressions, non-circular craters, and other likely volcanic vents. LPDs have a wide range of albedos and many are not as dark as previously thought. Most LPDs have intermediate albedos similar to those of mature low-titanium lunar maria.
2. Very Large or regional pyroclastic deposits, with spatial extents of 1000 to 50,000 km^2, are more numerous than has previously been thought; 20 Very Large deposits are identified in this analysis as compared to 10 in previous survey studies (Gaddis et al., 1985). This apparent increase in the number of deposits stems largely from improvements in data quality and analysis techniques for recognizing and characterizing LPDs.
3. Our results generally support previous research suggesting that size or areal extent of an LPD can be related to an inferred eruption style, with larger deposits formed by more continuous fire-fountaining from larger vents and smaller deposits by intermittently explosive vulcanian eruptions from smaller vents. However, the Very Large LPD at Oppenheimer NW, observed in a farside floor-fractured crater, appears to be an exception to this general case. Although described by Head et al. (2001) as the product of a vulcanian eruption, UVVIS spectral analyses of the Oppenheimer LPDs indicate that they resemble several Very Large LPDs in overall color, including possibly glass-rich deposits at Aristarchus, Humorum, and Dopplemayer. If the LPD at Oppenheimer NW has a substantial component of volcanic glass, then it would be unique among LPDs formed by vulcanian

eruption in having a recognizable major glass component.

4. Very Large LPDs have diverse compositions, but can generally be grouped into three classes.
   a. One class is distinctive and is dominated spectrally by black beads; this class is iron- and titanium-rich and includes deposits at Taurus–Littrow, Sinus Aestuum, Vaporum, and Rima Bode. Although many of these deposits are areally extensive, this black bead composition is limited to a few deposits in the central nearside of the Moon. These results suggest that the pyroclastic deposits most commonly recognized as having commercial potential, such as the black bead deposits at Taurus–Littrow that have been suggested as sources of oxygen, iron, and titanium (e.g., Hawke et al., 1990; Allen et al., 1996) may be restricted to a few source regions on the Moon.
   b. A second class, exemplified by Sulpicius Gallus, is similar to Apollo 17 deposits in overall composition and is likely to be titanium-rich, but may consist of a mixture of Fe^{2+}-bearing orange glasses and black beads that has a higher glass/bead ratio than that of Taurus–Littrow.
   c. A third class includes LPDs at Aristarchus, Harbinger, and Humorum and has pyroclastic material dominated by Fe^{2+}-bearing glasses; this class may have lower average titanium content and thus a different composition from most orange glasses observed at Taurus–Littrow. Because there are so few of these deposits, eruption of such glass-rich LPDs also appears to be a relatively rare event on the Moon.

5. Previous studies of smaller or localized LPDs by Hawke et al. (1989b) noted that one group (Group 1) of such deposits had near-infrared spectra that were interpreted as indicating the presence of significant highlands debris as well as more mafic material. In this analysis, many LPDs have spectral parameters that suggest the presence of significant highlands material. Such material may be entrained highlands wallrock or highlands contamination introduced into the LPD by lateral transport or vertical mixing.
6. Hawke et al. (1989b) also interpreted two groups (Groups 2 and 3 of that study) of smaller LPDs as containing a very large amount of mare basalt. Most of the Large, Medium, Small and Very Small LPDs investigated in this study have spectral parameters consistent with the presence of large amounts of mare basalt. These data suggest that the majority of LPDs may have had magmatic components that consisted of fragmented basalts, with substantial components of iron-bearing mafic minerals (clinopyroxene, olivine) and smaller amounts (if any) of iron-bearing volcanic glass.

References

Adams, J.B., Pieters, C., McCord, T.B., 1974. Orange glass: evidence for regional deposits of pyroclastic origin on the Moon, in: Proc. Lunar Sci. Conf. 5th, pp. 171–186.

Allen, C.C., Morris, R.V., McKay, D.S., 1996. Oxygen extraction from lunar soils and pyroclastic glass. J. Geophys. Res. 101, 26085–26095.

Arndt, J., Flad, K., Feth, M., 1979. Radiative cooling experiments on lunar glass analogues, in: Proc. Lunar Planet. Sci. Conf. 10th, pp. 355–373.

Arndt, J., von Englehardt, W., Gonzales-Cabeza, I., Meier, B., 1984. Formation of Apollo 15 green glass beads, in: Proc. Lunar Planet. Sci. Conf. 15th, J. Geophys. Res. 89, pp. C225–C232.

Baedeker, P.A., Chou, C.-L., Sundberg, L.L., Wasson, J.T., 1974. Volatile and siderophilic trace elements in the soils and rocks of Taurus–Littrow, in: Proc. Lunar Sci. Conf. 5th, pp. 1625–1643.

Blewett, D.T., Hawke, B.R., 2001. Remote sensing and geologic studies of the Hadley–Apennine region of the Moon. Meteorit. Planet. Sci. 26, 701–730.

Charette, M.P., McCord, T.B., Pieters, C.M., Adams, J.B., 1974. Application of remote spectral reflectance measurements to lunar geology classification and determination of titanium content of lunar soils. J. Geophys. Res. 79, 1605–1613.

Coombs, C.R., Hawke, B.R., 1992. Pyroclastic deposits on the western limb of the Moon, in: Proc. Lunar Planet. Sci. Conf. 22nd, pp. 303–312.

Coombs, C.R., Hawke, B.R., Lucey, P.G., 1990a. Pyroclastic deposits in the Nectaris region of the Moon. Lunar Planet. Sci. 21, 226–227.

Coombs, C.R., Hawke, B.R., Lucey, P.G., Owensby, P.D., Zisk, S.H., 1990b. The Alphonsus region: a geologic and remote sensing perspective, in: Proc. Lunar Planet. Sci. Conf. 20th, pp. 339–353.

Coombs, C.R., Allen, C.C., Hawke, B.R., 1998. Evaluation of Aristarchus plateau as a future lunar base site, in: Proc. Space 98. Am. Soc. Civ. Eng., pp. 608–615.

Delano, J.W., 1986. Pristine lunar glasses: criteria, data, and implications, in: Proc. Lunar Planet. Sci. Conf. 16th, Pt. 2, J. Geophys. Res. 91, D201–D213.

Eliason, E., Isbell, C., Lee, E., Becker, T., Gaddis, L., McEwen, A., Robinson, M., 1999. Mission to the Moon: the Clementine UVVIS global mosaic. PDS Volumes USA_NASA_PDS_CL_4001–4078.

Elphic, R.C., Lawrence, D.J., Feldman, W.C., Barraclough, B.L., Maurice, S., Binder, A.B., Lucey, P.G., 1998. Lunar Fe and Ti abundances: comparison of Lunar Prospector and Clementine data. Science 281, 1493–1496.

Gaddis, L.R., Pieters, C.M., Hawke, B.R., 1985. Remote sensing of lunar pyroclastic mantling deposits. Icarus 61, 461–489.

Gaddis, L., Hawke, B.R., Robinson, M.S., 1997. Analyses of three classes of small lunar pyroclastic deposits with Clementine data. Lunar Planet. Sci. 28, 389–390.

Gaddis, L., Rosanova, C., Hare, T., Hawke, B.R., Coombs, C., Robinson, M.S., 1998a. Small lunar pyroclastic deposits: a new global perspective. Lunar Planet. Sci. 29, 1807–1808.

Gaddis, L., Rosanova, C.R., Hawke, B.R., Coombs, C., Robinson, M., Sable, J., 1998b. Integrated multispectral and geophysical datasets: a global view of lunar pyroclastic deposits, in: New Views of the Moon, Lunar and Planetary Institute, Houston, TX, pp. 19–20.

Gaddis, L.R., Hawke, B.R., Robinson, M.S., Coombs, C.R., 1999. Juvenile materials in lunar pyroclastic deposits. Lunar Planet. Sci. 30, Abstract 1732.

Gaddis, L.R., Hawke, B.R., Robinson, M.S., Coombs, C., 2000. Compositional analyses of small lunar pyroclastic deposits using Clementine multispectral data. J. Geophys. Res. 105, 4245–4262.

Gaddis, L.R., Staid, M., Petro, N., 2001. Compositions of lunar pyroclastic deposits. Lunar Planet. Sci. 32, Abstract 1372.

Giguere, T.A., Taylor, G.J., Hawke, B.R., Lucey, P.G., 2000. The titanium contents of lunar mare basalts 2000. Meteoritics Planet. Sci. 35, 193–200.

Gillis, J.J., Jolliff, B.L., 2001a. Bimodal TiO_2 contents of mare basalts at Apollo and Luna sites and implications for TiO_2 derived from Clementine spectral reflectance. Lunar Planet. Sci. 32, Abstract 2164.

Gillis, J.J., Jolliff, B.L., 2001b. Integrating rock, soil, and remotely sensed TiO_2 concentrations yields a modified algorithm for calculating TiO_2 from Clementine UVVIS data and an improved global assessment of mare basalt TiO_2 distribution, submitted for publication.

Gillis, J.J., Jolliff, B.L., 2001c. New algorithm for mapping TiO_2 concentrations using Clementine UVVIS data suggests a non-uniform global distribution of basalt types, in: Eos, Trans. Am. Geophys. Union, Vol. 20, S240, Spring AGU, Boston, MA.

Gillis, J.J., Jolliff, B.L., Elphic, R.C., Maurice, S., Feldman, W.C., Lawrence, D.J., 2001. A hybrid method for calculating TiO_2 concentrations using Clementine UVVIS data, and verified with LunarProspector neutron spectrometer data. Lunar Planet. Sci. 32, Abstract 2185.

Hawke, B.R., MacLaskey, D., McCord, T.B., Adams, J.B., Head, J.W., Pieters, C.M., Zisk, S.H., 1979. Multispectral mapping of the Apollo 15-Apennine region: the identification and distribution of regional pyroclastics, in: Proc. Lunar Planet. Sci. Conf. 10th, pp. 2995–2934.

Hawke, B.R., Coombs, C.R., Lucey, P.G., 1989a. A remote sensing and geologic investigation of the Cruger region of the Moon, in: Proc. Lunar Planet. Sci. Conf. 19th, pp. 127–135.

Hawke, B.R., Coombs, C.R., Gaddis, L.R., Lucey, P.G., Owensby, P.D., 1989b. Remote sensing and geologic studies of localized dark mantle deposits on the Moon, in: Proc. Lunar Planet. Sci. Conf. 19th, pp. 255–268.

Hawke, B.R., Coombs, C.R., Clark, B., 1990. Ilmenite-rich pyroclastic deposits: an ideal lunar resource, in: Proc. Lunar Planet. Sci. Conf. 20th, pp. 249–258.

Hawke, B.R., Coombs, C.R., Campbell, B.A., Lucey, P.G., Peterson, C.A., Zisk, S.H., 1991. Remote sensing of regional pyroclastic deposits on the North Central portion of the lunar nearside, in: Proc. Lunar Planet. Sci. Conf. 21st, pp. 377–389.

Head, J.W., III, 1974. Lunar dark-mantle deposits: possible clues to the distribution of early mare deposits, in: Proc. Lunar Sci. Conf. 5th, pp. 207–222.

Head, J.W., III, Wilson, L., 1979. Alphonsus-type dark-halo craters: morphology, morphometry, and eruption conditions, in: Proc. Lunar Planet. Sci. Conf. 10th, pp. 2861–2897.

Head, J.W., III, Wilson, L., 1992. Lunar mare volcanism: stratigraphy, eruption conditions, and the evolution of secondary crusts. Geochim. Cosmochim. Acta 56, 2155–2175.

Head, J.W., III, Wilson, L., Pieters, C.M., 2001. Pyroclastic eruptions associated with the floor-fractured lunar farside crater Oppenheimer in the South Pole Aitken Basin, in: LPS XXXI, No. 1280.

Head, J.W., III, Wilson, L., Weitz, C.M., 2002. Dark ring in southwestern Orientale Basin: origin as a single pyroclastic eruption. J. Geophys. Res. 107, 10.1029/2000JE001438.

Heather, D.J., Dunkin, S., Wilson, L., 2001. Volcanism on the Marius Hills Plateau. Lunar Planet. Sci. 32, Abstract 1542.

Heiken, G., Vaniman, D., French, B.M. (Eds.), 1991. Lunar Sourcebook. Cambridge Univ. Press, New York, p. 205.

Heiken, G.H., McKay, D.S., Brown, R.W., 1974. Lunar deposits of possible pyroclastic origin. Geochim. Cosmochim. Acta 38, 1703–1718.

Hiesinger, H., Jaumann, R., Neukum, G., Head, J.W., III, 2000. Ages of mare basalts on the lunar nearside. J. Geophys. Res. 105, 29239–29275.

Hiesinger, H., Head, J.W., III, Wolf, U., Neukum, G., 2001. New age determinations of lunar mare basalts in Mare Cognitum, Mare Nubium, Oceanus Procellarum and other nearside mare. Lunar Planet. Sci. 32, Abstract 1815.

Howard, K.A., Carr, M.H., Muehlberger, W.R., 1973. Basalt Stratigraphy of Southern Serenitatis, Apollo 17 Prelim. Sci. Rep. NASA SP-330, pp. 29.1–29.13.

Johnson, J.R., Larson, S., Singer, R., 1991. Remote sensing of potential lunar resources 1. Near-side compositional properties. J. Geophys. Res. 96, 18861–18882.

Lawrence, D.J., Feldman, W.C., Barraclough, B.L., Binder, A.B., Elphic, R.C., Maurice, S., Thomsen, D.R., 1998. Global elemental maps of the Moon: the Lunar Prospector gammaray spectrometer. Science 281, 1484–1489.

Lucchitta, B.K., 1978. Geologic Map of the North Side of the Moon, USGS Map 1–1062 (1:5,000,000 scale).

Lucchitta, B.K., Sanchez, A.G., 1975. Crater studies in the Apollo 17 region, in: Proc. Lunar. Sci. Conf. 6th, pp. 2427–2441.

Lucchitta, B.K., Schmitt, H.H., 1974. Orange material in the Sulpicius Gallus formation at the southwestern edge of Mare Serenitatis, in: Proc. Lunar Sci. Conf. 5th, pp. 223–234.

Lucey, P.G., Hawke, B.R., Pieters, C.M., Head, J.W., McCord, T.B., 1986. A compositional study of the Aristarchus region of the Moon using near-infrared reflectance spectroscopy. J. Geophys. Res. 91, D344–D354.

McCord, T.B., Clark, R.N., Hawke, B.R., McFadden, L.A., Owensby, P.D., Pieters, C.M., Adams, J.B., 1981. Moon: near-infrared spectral reflectance, a first good look. J. Geophys. Res. 86, 10883–10892.

Papike, J.J., Ryder, G., Shearer, C.K., 1998. Lunar samples, in: Planetary Materials, chap. 5, Revi. Miner. 36, 5.1–5.234.

Petro, N.E., Gaddis, L.R., Staid, M.I., 2001. Analysis of the Oppenheimer pyroclastic deposits using Clementine UVVIS data. Lunar Planet. Sci. 32, Abstract 1953.

Pieters, C.M., 1978. Mare basalt types on the front side of the Moon: a summary of spectral reflectance data, in: Proc. Lunar Planet. Sci. Conf. 9th, pp. 2825–2849.

Pieters, C.M., 1993. Compositional diversity and stratigraphy of the lunar crust derived from reflectance spectroscopy, Ch. 14, in: Pieters, C.M., Englert, P.A.J. (Eds.), Remote Geochemical Analysis: Elemental and Mineralogical Composition, Cambridge Univ. Press, Cambridge, UK, pp. 309–339.

Pieters, C.M., McCord, T.B., Zisk, S.H., Adams, J.B., 1973. Lunar black spots and the nature of the Apollo 17 landing area. J. Geophys. Res. 78, 5867–5875.

Pieters, C.M., McCord, T.B., Charette, M.P., Adams, J.B., 1974. Lunar surface: identification of the dark mantling material in the Apollo 17 soil samples. Science 183, 1191–1194.

Pieters, C.M., Head, J.W., Sunshine, J.M., Fischer, E.M., Murchie, S.L., Belton, M., McEwen, A., Gaddis, L., Greeley, R., Neukum, G., Jaumann, R., Hoffmann, H., 1993. Crustal diversity of the Moon: compositional analyses of Galileo SSI data. J. Geophys. Res. 98, 17127–17148.

Pieters, C.M., Taylor, L.A., McKay, D., Wentworth, S., Morris, R., Keller, L., 2000. Spectral characterization of lunar mare soils. Lunar Planet. Sci. 31, Abstract 1865.

Prettyman, T.H., Feldman, W.C., Lawrence, D.J., McKinney, G.W., Binder, A.B., Elphic, R.C., Gasnault, O.M., Maurice, S., Moore, K.R., 2002. Library least squares analysis of Lunar Prospector gamma ray spectra. Lunar Planet. Sci. 33, Abstract 2012.

Rosanova, C., Gaddis, L., Hare, T.M., Coombs, C., Hawke, B.R., Robinson, S., 1998. Characterization of "new" pyroclastic deposits on the Moon using Clementine data. Lunar Planet. Sci. 29, 1710–1711.

Scott, D.H., McCauley, J.F., West, M.N., 1977. Geologic Map of the West Side of the Moon, USGS Map 1-1034 (1:5,000,000 scale).

Shearer, C.K., Papike, J.J., 1993. Basaltic magmatism on the Moon: a perspective from volcanic picritic glass beads. Geochim. Cosmochim. Acta 57, 4785–4812.

Solomon, S.C., Comer, R.P., Head, J.W., III, 1982. The evolution of impact basins: viscous relaxation of topographic relief. J. Geophys. Res. 87, 3975–3992.

Spudis, P.D., 1989, Young dark mantle deposits on the Moon, in: NASA TM 4210, pp. 406–407.

Staid, M.I., 2000. Remote Determination of the Mineralogy and Optical Alteration of Lunar Basalts Using Clementine Multispectral Images: Global Comparisons of Mare Volcanism, Ph.D. Thesis. Brown University, Providence, RI.

Staid, M.I., Pieters, C.M., 2000. Integrated spectral analysis of mare soils and craters: applications to eastern nearside basalts. Icarus 145, 122–139.

Staid, M.I., Pieters, C.M., 2001. Mineralogy of the last lunar basalts: results from Clementine. J. Geophys. Res. 106, 27887–27900.

Tera, F., Wasserburg, G.J., 1976. Lunar ball games and other sports, in: Lunar Science VII, Abstracts of Papers Submitted to the Seventh Lunar Science Conference, pp. 858–860.

Uhlmann, D.R., Klein, L., Kritchevsky, G., Hopper, R.W., 1974. The formation of lunar glasses, in: Proc. Lunar Sci. Conf. 5th, pp. 2317–2331.

Weitz, C.A., Head, J.W., III, Pieters, C.M., 1998. Lunar regional dark mantle deposits: geologic, multispectral, and modeling studies. J. Geophys. Res. 103, 22725–22759.

Whitford-Stark, J.L., 1990. The volcanotectonic evolution of Mare Frigoris, in: Proc. Lunar Planet. Sci. Conf., 20th, pp. 175–185.

Whitford-Stark, J.L., Head III, J.W., 1980. Stratigraphy of Oceanus Procellarum basalts: sources and styles of emplacement. J. Geophys. Res. 85, 6579–6609.

Wilhelms, D.E., 1987. The Geologic History of the Moon, USGS Prof. Paper 1348.

Wilhelms, D.E., El-Baz, F., 1977. Geologic Map of the East Side of the Moon, USGS Map 1948 (1:5,000,000 scale).

Wilhelms, D.E., McCauley, J.F., 1971. Geologic Map of the Near Side of the Moon, USGS Map 1-703 (1:5,000,000 scale).

Wilhelms, D.E., Howard, K.A., Wilshire, H.G., 1979. Geologic Map of the South Side of the Moon, USGS Map 1-1162 (1:5,000,000 scale).

Wilson, L.W., Head III, J.W., 1981. Ascent and eruption of basaltic magma on the Earth and Moon. J. Geophys. Res. 86, 2971–3001.

Zisk, S.H., Hodges, C.A., Moore, H.J., Shorthill, R.W., Thompson, T.W., Whitaker, E.A., Wilhelms, D.E., 1977. The Aristarchus–Harbinger region of the Moon: surface geology and history from recent remote-sensing observations. The Moon 17, 59–99.

Zuber, M.T., Smith, D.E., Lemoine, F.G., Neumann, G.A., 1994. The shape and internal structure of the Moon from the Clementine Mission. Science 266, 1839–1843.